Chapter 18

Advances in Amazonian Biogeochemistry

K. O. Konhauser[1], W. S. Fyfe[1], W. Zang[1], M. I. Bird[2], and B. I. Kronberg[3]

[1]Department of Earth Sciences, University of Western Ontario, London, Ontario N6A 5B7, Canada
[2]Research School of Earth Sciences, The Australian National University, GPO Box 4, Canberra 2601, Australia
[3]Geology Department, Lakehead University, Thunder Bay, Ontario P7B 5E1, Canada

Recent observations on the geochemistry, biogeochemistry and stable isotope systematics of waters, soils and sediments of the Amazon region indicate the profound influence of biological processes on the nature of the surface and near surface materials. These same materials provide evidence for major change in vegetation types and climate during the recent past.

The chemistry of local soils and waters provides key indicators of the agricultural and mineral resource potential of various regions. The extremely deep bio-weathering in the Amazon system has produced many important and new types of mineral deposits. In regions of intense and deep leaching, the input of many chemical species may be dominated by rain and aerosols.

Multiple Fluxes Influencing Amazonian River Chemistry

The Amazon River Basin is the largest modern river system in terms of drainage area (6 million km^2), supplying ~20% of fresh water to the world's oceans (5.5 x 10^{12} m^3/year, Villa Nova et al.) (*1*) and discharging ~10^9 metric tons of sediment to the Atlantic Ocean (Meade et al.) (*2,3*). The system's headwaters begin within a few hundred kilometres of the Pacific Ocean and its tributaries extend for hundreds of kilometres throughout central South America. The entire Basin may be divided into the mountainous Andean regions and the much more extensive lower basins. Chemical signatures of surface soils and sediments in lower Amazonia show these materials have undergone intense chemical weathering, while, in the Andes Mountains, weathered material is still being generated.

Early studies in the Amazon Basin showed that the waters were chemically and physically very heterogeneous. The first classification of Amazonian rivers was based on their physical appearance (*4*). Whitewater rivers are rich in dissolved

0097–6156/95/0588–0208$17.00/0

solutes and are extremely turbid owing to their high concentrations of suspended sediment. Blackwater rivers are relatively infertile rivers characterized by low sediment yields and their "tea-colored" (*5*) acidic waters that are rich in dissolved humic material derived from decaying surface vegetation (*6,7*). Finally, clearwater rivers are relatively transparent, green-colored rivers that are neither turbid with detrital materials or colored by humic compounds (*8*).

The chemistry of Amazonian rivers have long been attributed both to the variability of the geological source and to the erosional regime through which the rivers flow. Early studies by Raimondi (*9*) and Katzer (*10*) observed that the low dissolved inorganic concentrations in some lowland rivers contrasted with those of rivers draining the Andes Mountains. It was later shown that the rivers flowing through the central lowlands were typically blackwater in composition, whitewater streams were distinctive of the waters draining the Andes, while clearwater types were characteristic of rivers originating in the Precambrian shields (*11-13*).

More recently, several papers have begun to deal specifically with the elemental composition of Amazonian rivers (*13-20*). Studies such as Stallard and Edmond (*13*) have indicated that the distribution of major cations and anions in the dissolved load were controlled by substrate lithology in the source regions. This relationship was later extended to several trace elements (*20*). The chemistry of rivers in the Amazon Basin have also been attributed to the atmospheric precipitation of cyclic salts (*14*) with the ratios of major dissolved ions in lowland rivers (which are similar to sea salt) indicative of a marine origin. Despite the compilation of published work on the chemistry of Amazonian waters, most studies have dealt specifically with 1) a limited number of major elements and trace metals, and 2) the impact of geologic, geochemical, and petrographic properties of the source regions on the chemical composition of surface waters. While weathering is undoubtedly of fundamental importance in the supply of solutes to a river system, this study suggests that other factors also have impact on Amazonian river chemistry.

Influence of Soil Geochemistry and Mineralogy. Since the earliest studies on Amazonian river chemistry, it has become apparent that the chemical and physical variability exhibited by surface waters were largely attributed to geologic heterogeneity of the Amazon Basin. On the basis of distinct differences in geology, soil types, and vegetation, Fittkau et al., (*21*) have divided the Amazon Basin into three major geochemical provinces (Figure 1): the western peripheral region, where soils (known as the varzea) and waters are fertile, the Central Amazon, an area where the soils and waters are deficient in nutrients, and the northern and southern peripheral regions (Precambrian Shields) with intermediate compositions (*20*).

Based on similarities between the major cation and trace metal levels in the soil samples (Table I), and the dissolved metal concentrations in surface waters flowing through the varzea, the Central Amazon, and the Shields (Figure 2), our research confirms that the rivers were in chemical equilibrium with their drainage

Table I. Average Chemical Composition of Soils in Study Areas with Crustal Abundance

	Crustal Abundance	Central Amazon	Shield	Varzea
SiO_2	58.50	70.22	51.78	63.05
TiO_2	1.05	0.62	1.17	...0.88
Al_2O_3	15.80	16.66	17.15	.15.47
Fe_2O_3	6.50	2.79	19.02	5.87
MnO	0.14	0.02	0.14	0.10
MgO	4.57	0.18	0.26	1.75
CaO	6.51	0.00	0.06	1.38
K_2O	2.22	0.04	0.22	2.21
P_2O_5	0.25	0.04	0.10	0.18
Na_2O	3.06	0.00	0.02	1.25
Nb	11.00	19.75	19.50	16.00
Zr	100.00	600.25	361.50	330.00
Y	20.00	8.65	25.75	39.00
Sr	260.00	9.50	22.13	214.50
Rb	32.00	5.20	15.95	99.00
Pb	8.00	<13.50	13.45	21.50
Zn	80.00	<9.75	28.75	91.75
Cu	75.00	<8.13	363.00	27.25
Ni	105.00	6.85	17.25	30.25
Co	29.00	<5.00	20.50	16.75
Cr	185.00	113.50	161.50	58.50
Ba	250.00	51.25	66.50	466.25
V	230.00	32.00	231.75	100.75
As	1.00	<5.00	16.25	<8.20
Ga	18.00	14.25	24.50	20.25
U	0.91	<3.50	<6.25	<5.00
Th	3.50	14.25	<27.75	<9.00

Major oxide compositions (in wt.%) and trace metal compositions (in Og/g). Values from Konhauser et al. (*22*). Crustal abundances are from Fairbridge (*23*) and Taylor and McLennan (*24*). Averages with "<" indicate concentrations below given value.

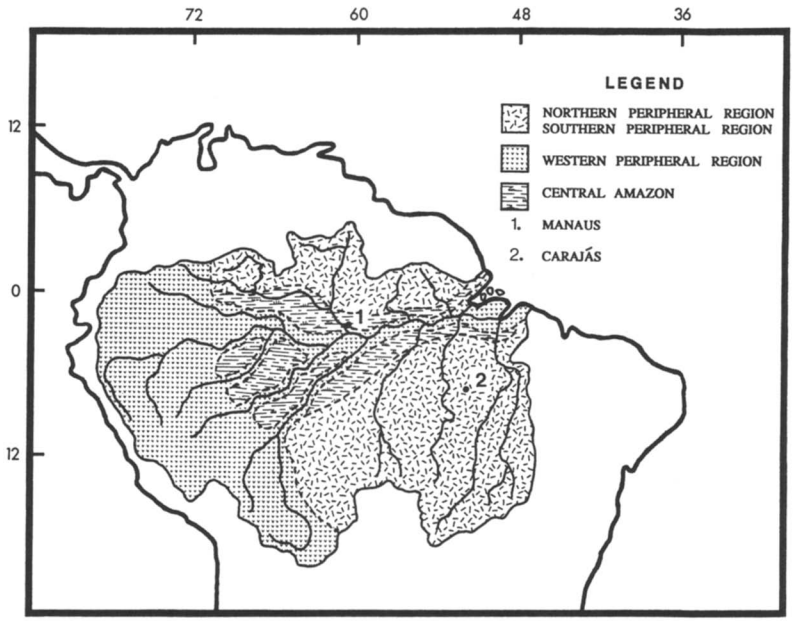

Figure 1. The major geochemical provinces of the Amazon Basin, after Fittkau et al. (*21*). Location of the study areas in Manaus and Carajás are shown (*25*).

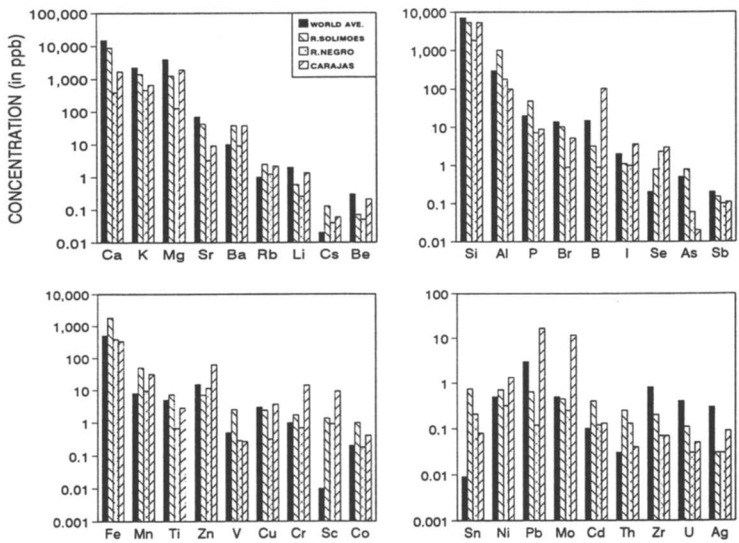

Figure 2. Comparison of dissolved metal concentrations in surface waters of the Rio Solimões, the Rio Negro, and forested streams in Carajás with world river average (*25*).

basins (*25*). In geologically active areas, such as the Andes Mountains, crustal elements such as Si, Al, K, Na, Ca, Be, Li, Zn, Mo, F, and B are mixed with newly extruded mantle elements such as Ca, Mg, Cu, Co, Ni, S, V, Cr, and Se (*26*). With high rates of erosion of the varied lithologies in the source regions, enormous quantities of unweathered minerals (feldspar and mica), metal-rich clays (smectite, chlorite, and illite), and dissolved metals are transported downstream by whitewater rivers (*25*), resulting in the fertile soils of the varzea that are almost exclusively derived from the annual deposition of new sediments during seasonal floods (*12*). The chemistry of the dissolved size fraction in the Rio Solimões, therefore, reflects the substrate lithology in the Andes, with the high concentration of calcium, for example, indicative of a limestone source (*13*), while continuous leaching of the varzea soils further supplies the solute-rich river with additional metals.

The high concentration of dissolved metals in the Rio Solimões is contrasted by the solute-deficient waters of the Rio Negro which drains the highly weathered lateritic and podsolitic terrains of the Central Amazon. Due to a lack of exposed rock, the intense chemical weathering of the humid tropics over millions of years, and the low rates of weathering in conjunction with the development of thick, siliceous and aluminous soils, the suspended sediment are typically cation-depleted, consisting almost entirely of quartz and kaolinite (*27*), while the dissolved load is dominated by silicon, with extremely low levels of major cations and trace metals.

Rivers that drain the Precambrian Shield typically carry a limited suspended and dissolved load (*28*), reflecting the tectonic stability which leads to low erosional rates and high leaching (*26*). Furthermore, in these stable cratonic regions, which are favored by sedimentary rocks such as orthoquartzites, with no nutrients, or granitic and metamorphic rocks, with a limited nutrient spectrum and low erosional rate (*27*), the soils are typically depleted in nutrients. Although these conditions should give rise to extremely solute-deficient rivers, the waters flowing through Carajás have an intermediate composition. This discrepancy may largely reflect the fact that Carajás is a very metallogenic area, rich in mineral deposits (*29*), which upon weathering could supply dissolved metals to local river systems.

These observations, collectively, suggest that we should be able to classify the chemical composition of rivers according to the geochemistry and mineralogy of the soils through which they flow. This has profound implications for using water chemisty as an indicator of the agricultural and mineral potential of a region. A comparison of three key macronutrients and the total dissolved inorganic solids (TDS) of several great rivers of the world speak eloquently about the state of the soils (Table II). The Danube, Mississippi, Yangtze, and Nile river systems all have high dissolved metal concentrations, reflecting the young, fertile soils through which they flow. Since plants require a wide range of macronutrients and micronutrients, their solute-rich waters indicate a high capacity to support bioproductivity. In contrast, the extremely low concentration of dissolved metals in the waters of the Rio Negro is indicative of the poor nutrient status of the Central Amazon. The inability of the lateritic soils to support agricultural activity (*26*) is

probably the reason why historically this region has never been overpopulated by humans (*30*). Therefore, in regions such as the Central Amazon, chemical analyses of the river systems should reflect the incapability of the soils to sustain long-term crop production. Clearly then, using river chemistry as an agricultural indicator would be a very efficient way of assuring soil potential prior to massive development projects.

Table II. Comparison of Dissolved Solutes in Principal World Rivers (in μg/L)

	Ca	*Mg*	*K*	*TDS*
Danube	49.0	9.0	1.0	265.0
Mississippi	39.0	10.7	2.8	265.0
Yangtze	45.0	6.4	1.2	232.0
Nile	25.0	7.0	4.0	225.0
Lower Negro	0.4	0.1	0.5	3.4

"World river values from ref. 31".

Knowing the chemical composition of a river system may also be of use in determining the mineral potential of a region. The high concentration of a number of metals (such as Zn, Cu, Cr, Ni, Pb, Mo, Co, Mn, Rb, Ba, B, I, and Se) in the waters draining the Shield areas in Carajás (relative to both Amazonian rivers and world river average) confirms the presence of one of the greatest mining areas of the modern world. While the high aqueous concentration of some of these metals may be associated with local mining activity, many of these rivers drain completely forested areas with no anthropogenic influence. Under these conditions, river chemistry may be useful in mineral exploration.

Impact of Microbial Metal Sorption and Biomineralization. Many of the chemical processes occurring within aqueous systems have been shown to be biologically mediated. Although all forms of life possess some characteristics that make them biogeochemically important, much of the focus today is being directed towards the role of microorganisms, such as bacteria and algae, in the cycling of elements. Their significance arises from their ability to not only live in an unparalleled variety of environments, but also their ability to change their surroundings.

In most aquatic systems, the majority of microbial activity appears to be associated with submerged solid surfaces (*32*). The complex microbial communities that develop on substrata are commonly referred to as biofilms, and consist of a consortia of bacteria, cyanobacteria, and algae held firmly together in a highly hydrated polymeric matrix of polysaccharides extruded by the cells (*33*). The formation of biofilms is generally regarded as a growth strategy that affords attached cells with a survival advantage not available to free-living cells (*33*). Benthic microorganisms benefit not only from protection against the high shear of

turbulent flow (*34*), but also through the elevated concentrations of organic and inorganic compounds that accumulate at solid-liquid interfaces (*35*).

In order to utilize essential metallic ions as nutrients for growth, microorganisms must have the ability to adsorb and concentrate metal cations from solution. In many microorganisms, this may be accomplished, in part, through electrostatic interactions with reactive acidic groups (carboxyl and phosphoryl) contained within the constituent polymers of microbial cell walls (*36,37*). A number of experimental studies have clearly demonstrated that substantial quantities of various metals can be bound and accumulated by a variety of bacterial cells (*38-40*), whereas Kuyucak and Volesky (*41*) have shown that the cellulosic materials in filamentous algae played an important role in the biosorption of gold.

Microbial mediated physiological processes can also have profound effects on the precipitation of mineral phases. In bacteria biominerals are commonly generated as secondary events from interactions between the activity of the microorganisms and its surrounding environment (*42*). Based on the inherent metal-binding capacity of the anionic structural polymers that reside in the cell-wall fabric, Beveridge and Murray (*39*) have proposed a two-step mechanism for the development of authigenic mineral phases in association with bacterial cells. The first step involves a stoichiometric interaction between metals in solution with the cell's reactive chemical groups. Once bound to the bacteria, these metals can then serve as nucleation sites for the deposition of more metal ions from solution. The end result is a mineralized cellular matrix that contains detectable concentrations of metal ions that are not easily solubilized (*43*). In contrast, unicellular algae, such as diatoms, are examples of biologically-controlled mineralizers that remove silicon to fulfill physiological functions such as DNA synthesis and to form their siliceous skeletons (*44*). This process of biomineralization is characterized by the development of an organic framework or mold into which various ions are actively introduced. During biologically controlled mineralization an area is sealed off from the environment allowing specific ions of choice (e.g., Si) to diffuse into the space delineated for mineral precipitation. The cell therefore, creates an internal environment completely independent of the external conditions. It is under these "ideal" conditions that mineralization may occur (*45*).

The role of bacteria. In a recent study on the activity of benthic bacteria in Amazonian rivers (*22*), microbial biofilms were collected off of submerged plants and sediment, and subsequently analyzed with transmission electron microscopy (TEM), coupled with energy dispersion X-ray spectroscopy (EDS) and selected area electron diffraction (SAED). With TEM, it was observed that bacterial biomineralization involved a complex interaction between metals in solution with the reactive components of the cell. The anionically-charged cell wall and the encompassing layers provided special microenvironments for the deposition of iron and other soluble cationic species. Ferric iron, which exhibits unstable aqueous chemistries, was bound in significant amounts, and previous studies indicate that

this may be sufficient to induce transformations to the insoluble hydroxide form (e.g. ferrihydrite) (*46*).

Through progressive mineralization, bound iron served as nucleation sites for the precipitation and growth of the complex (Fe, Al) - silicates (Figures 3, 4A). It is likely that the initial (Fe, Al) - silicate phases precipitated directly through the reaction of dissolved silicon and aluminum to the bound metallic cations, with continued aggregation of these hydrous precursors resulting in the formation of low-order, amorphous phases that are characterized by large surface areas with a high adsorptive affinity for additional metal cations (*47*). Because they lack a regular crystal structure, these hydrous compounds are unstable and will, over time dehydrate, converting to more stable crystalline forms. In our study area, the hydrous chamosite-like clay appeared especially reactive to silicic acid (H_4SiO_4). Continued adsorption of silicon, through hydrogen bonding of the hydroxyl groups in the bound cations with the hydroxyl groups in the soluble silica seems to have accompanied the conversion of the low-order phase to the crystalline phase (*48*). Eventually this process led to the complete encrustation of the bacterial cell within a mineralized matrix.

It is an interesting observation that all bacterial populations examined in the Rio Solimões consistently formed identical mineral phases. This suggested that the bacteria from our sampling area, regardless of their physiology, were capable of serving as passive nucleation sites for (Fe, Al) - silicate precipitation. Conversely, all bacteria from the Rio Negro showed a conspicuous absence of mineralization (Figure 4B).

It is clear then, that the differences in mineral accumulation exhibited by bacterial cells in the Rio Solimões and the Rio Negro must reflect differences in the physical and chemical conditions of their riverine environments. The Rio Solimões is a fertile river, rich in suspended sediments and dissolved inorganic solutes. As a result, the bacteria will have an abundant supply of metals in solution with which to complex and to accumulate. In contrast, the Rio Negro is an extremely infertile river characterized by low levels of major cations and trace metals. With very dilute waters, the bacteria presumably are unable to bind sufficient quantities of metals to form authigenic mineral phases, suggesting that both metal sorption and biomineralization largely reflect the availability of dissolved solutes in the water column.

In a solute-rich river system such as the Rio Solimões, the fate of the metal-loaded bacteria may have profound implications for the transfer of metals from the hydrosphere to the sediment (*49*). Given that planktonic bacterial populations in the Rio Solimões are typically on the order of 1×10^6 to 4×10^6 cells/ml (*50*), it is not difficult to imagine that these microorganisms could effectively cleanse the water of dilute metals and partition them into the sediments (*43*). Furthermore, in the microenvironment overlying a biofilm, the aqueous chemistry will be altered by the activity of the microorganisms present. Although this water layer is very thin, when one takes into consideration the large surface area of solid substratum on a river's bed that is colonized by biofilms, the volume of water that falls directly

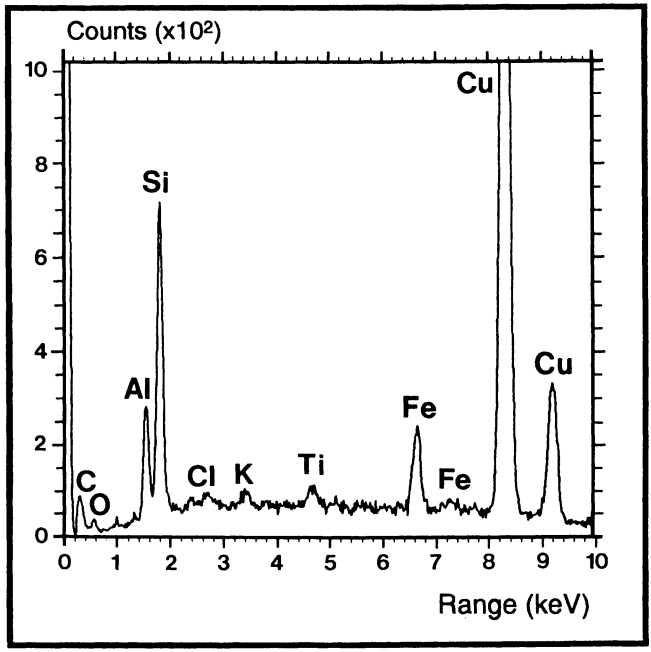

Figure 3. EDS spectra of the crystalline grains associated with epiphytic bacterial cells from the Rio Solimões. Cu peaks are from the supporting grid and the Cl peak is due to contamination from the embedding material (EPON).

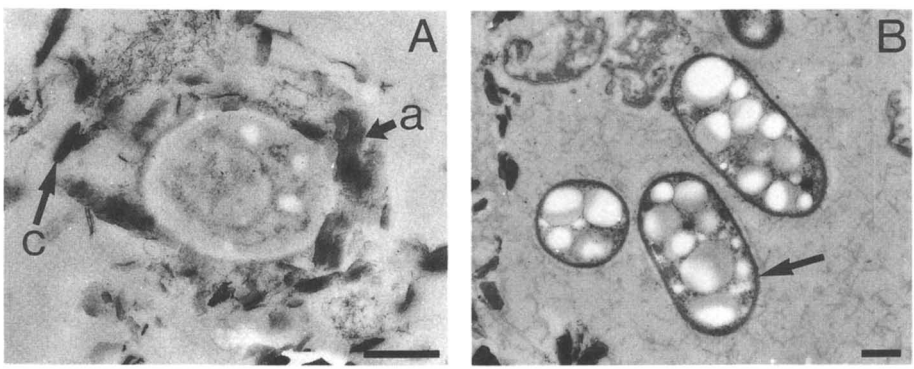

Figure 4. TEM image of (A) a completely encrusted epiphytic bacterial cell (stained with uranyl acetate and lead citrate) from the Rio Solimoes, with a complete range of morphologies including the amorphous, low-order phases (a), transition phases (t), and crystalline phases (c) and: (B) a small colony of epiphytic bacteria (stained) from the Rio Negro, loosely encapsulated by organic material. Arrow indicates the low levels of mineralization on the outer cell wall. Scale bar = 400 nm.

under microbial influence is substantial. In this regard, biofilms dominate the reactivity of the water-substrate interface and influence the transfer of metals from the hydrosphere to the sediment. Through diagenesis, the bound metals may also become immobilized as stable mineral phases and collect as sediment, suggesting the importance of microorganisms in metal deposition, low temperature clay formation, and, invariably, mudstone diagenesis.

The role of algae. Filamentous algal samples collected from different riverine environments in both the Manaus and Carajás areas indicated that metals were consistently removed from the waters by these eucaryotic microorganisms (*51*). The pattern which seems to arise is that algae effectively sequester and concentrate the metals available to them within their aqueous environment (Table III). Some metals are extracted from their surrounding environment to fulfill essential physiological functions, whereas the adsorption of other metals, without known cellular functions, largely reflects the strong complexing ability of the reactive organic components of the living cell.

If we conclude that metal concentrations within the algal biomass are a direct reflection of availability, then it is not surprising that the concentration of metals in the filamentous algae of the Rio Solimões greatly exceeded those of the Rio Negro. A similar relationship of metal concentration also arises between algal samples obtained from forested and completely deforested regions. Tropical plant species have adapted over millions of years to the highly leached and weathered soils of the tropics by developing a closed system that effectively conserves and recycles needed nutrients (*52*). Under these forested conditions the river system is continuously supplied with nutrients through the slow leaching from leaves, soils, and decaying organic matter. Removal of the vegetation through logging and slash-and-burn agricultural practices, however, disrupts the nutrient-conserving mechanisms through increased soil erosion. Over time this causes the level of soil nutrients to fall below the level of an undisturbed forest (*52*), with nutrient inputs into the river systems becoming minimal. This situation appears consistent with the data from these algal samples which show a higher metal concentration in the microorganisms from the forested streams.

The role of algae in biogeochemical cycling extends beyond trace metal extraction. Siliceous microorganisms, such as the diatoms, are commonly the most abundant freshwater eucaryotic microorganisms, and the development of large populations is invariably accompanied by a marked decline in the amount of dissolved silicon from the waters in rivers (*53*) and lakes (*54*). This situation is consistent with the surface waters of the Rio Negro, where the dissolved silicon levels were a maximum of 2100 μg/L. Despite low silicon levels, which are characteristic of Central Amazon rivers, the waters from the Rio Negro were capable of supporting prolific diatom growth, with scanning electron microscopy (SEM) indicating that submerged wood (Figure 5A), rocks, and leaves served as their solid substrates for growth (*55*).

Table III. Average Chemical Composition of Waters and Algae in Amazonian Rivers

	Rio Negro			*Rio Solimões*			*Forested*			*Deforested*		
	Water (ug/L)	*Algae* (ug/g)	*Conc. Factor*	*Water* (ug/L)	*Algae* (ug/g)	*Conc. Factor*	*Water* (ug/L)	*Algae* (ug/g)	*Conc. Factor*	*Water* (ug/L)	*Algae* (ug/g)	*Conc. Factor*
Ti	0,68	336,25	494.485	7,37	5850,00	793.758	2,86	3677,50	1.285.839	3,00	1233,33	411.111
V	0,29	12,80	44.138	2,52	210,00	83.333	0,27	108,25	400.926	0,50	70,33	141.801
Cr	0,69	9,63	13.960	1,73	141,75	81.936	14,16	86,65	6.119	12,20	48,67	3.989
Mn	9,63	87,25	9.060	50,13	8400,00	167.564	31,25	3200,00	102.400	403,67	3600,00	8.918
Fe	385,00	9475,00	24.610	1796,25	65500,00	36.465	331,00	54500,00	164.653	1596,67	52666,67	32.985
Co	0,18	1,98	10.972	1,00	57,00	57.000	0,41	92,50	225.610	2,09	57,00	27.273
Ni	0,32	4,20	13.125	0,71	67,00	94.366	1,33	66,75	50.188	2,11	32,00	15.166
Cu	0,32	7,33	22.891	2,40	94,75	39.479	3,70	309,75	83.716	8,73	80,67	9.240
Zn	11,54	48,75	4.224	7,10	207,50	29.225	61,26	150,75	2.461	170,00	138,00	812
As	0,06	1,00	16.625	0,79	26,25	33.228	0,02	7,56	377.750	0,81	6,90	8.487
Zr	0,07	8,33	118.929	0,20	108,00	540.000	0,07	154,75	2.210.714	0,06	31,67	558.495
Mo	0,25	0,72	2.890	0,45	2,53	5.611	11,61	2,20	189	0,17	2,94	17.711
Ag	0,03	0,66	21.892	0,03	6,02	200.500	0,09	0,71	7.867	0,07	0,24	3.381
Cd	0,12	0,10	863	0,40	2,11	5.281	0,13	0,41	3.173	0,15	1,30	8.475
Sn	0,21	0,55	2.607	0,75	3,85	5.133	0,08	3,09	38.594	0,08	2,10	27.632
Hg	0,17	0,09	506	0,12	0,46	3.813	0,25	0,18	711	0,24	0,18	774
Pb	0,12	7,75	64.583	0,64	39,25	61.328	16,51	8,60	521	6,27	11,90	1.898
U	0,03	0,48	16.000	0,11	4,65	42.273	0,05	5,03	100.500	0,37	3,00	8.174

Note: conc. factor = concentrations of metal in algae/concentration of metal in water. Values from Konhauser and Fyfe (*51*)

Seidl et al.; Chemistry of the Amazon
ACS Symposium Series; American Chemical Society: Washington, DC, 1995.

In accordance with low weathering rates exhibited in the Central Amazon, the source of silicon for diatom growth is largely sustained through the recycling of biogenic silica (*56*). The recycling of silicon in diatoms involves the dissolution of opaline skeletons and subsequent biological uptake. Sediment samples collected along the Rio Negro indicated the ubiquitous presence of diatom fragments which served as a major source of dissolving silica. Furthermore, within the small tributaries and flooded forests of the Rio Negro where benthic communities (e.g. *Navicula* sp.) are abundant, dissolution began in situ on the substratum. Upon death of the microorganism, the remnant siliceous frustules became fragmented, partially dissolving, and within micrometres to millimetres of the surface, reprecipitated as textureless, siliceous overgrowths (Figure 5B). These amorphous overgrowths are formed when the dissolved silicon levels become locally supersaturated before opal-A dissolution has gone to completion (*57*). Dissolution, therefore, becomes interrupted by the re-precipitation of a less soluble, nonbiogenic, siliceous ooze referred to as opal-A (*58,59*).

This dissolution-reprecipitation process may also alter the structure of the wood sample. The ubiquitous nature of the diatoms and the precipitation of the silica gel suggested that the wood samples were undergoing a void-filling process of silicification (*60*). In our samples this process began with the dissolution of diatoms on the surface and within. The silicic acid produced from the dissolving frustules may permeate throughout the wood. Hydrogen bonding between the hydroxyl groups in the silicic acid and the hydroxyl groups in the cellulose then leads to the deposition of opaline silica on the surfaces of individual wood cells (*60*). It is, therefore, no surprise to see a siliceous gel, both on the wood surface and within the wood.

The extent of this silicification process may be significant when the vast number of partially submerged trees in the study area is considered. The slow flowing movement of water within the flooded forests and the preferential attachment of diatoms to the outer wood surfaces may allow for silicon levels to build up sufficiently in microenvironments. Therefore, many of the trees within these flooded forests potentially can become reservoirs of highly reactive silica, disrupting the amount of silicon locally recycled through the freshwater system.

Metal Complexation by Organic Materials. Most studies of biogenic materials in Amazonian rivers have been confined to bulk measurements of the concentration of particulate organic carbon (POC) and dissolved organic carbon (DOC), traditionally defined by separation with a 0.5 μm filter (*61*). The POC is largely unreactive, and consists of a coarse fraction (>63 μm) comprised of tree leaf debris and some wood, with the fine fraction (<63 μm) derived primarily from soils and grasses (*5*). The DOC consists predominantly of humic substances, such as humic acids (HA) and fulvic acids (FA) (*62*). These humic substances are generally thought to be refractory, terrestrially derived organic matter leached from the surrounding soils (*63*). The remaining DOC includes potentially labile biochemical components such as proteins and carbohydrates (*64*).

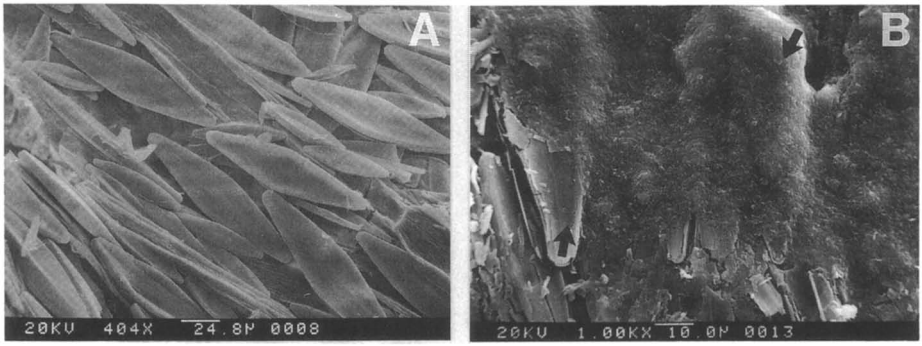

Figure 5. SEM images of (A) diatoms (*Navicula* sp.) on outer wood surface, collected upstream of Manaus on the Rio Negro and (B) the outer wood surface covered by a textureless, siliceous gel. Arrows indicate remnant frustule and siliceous gel.

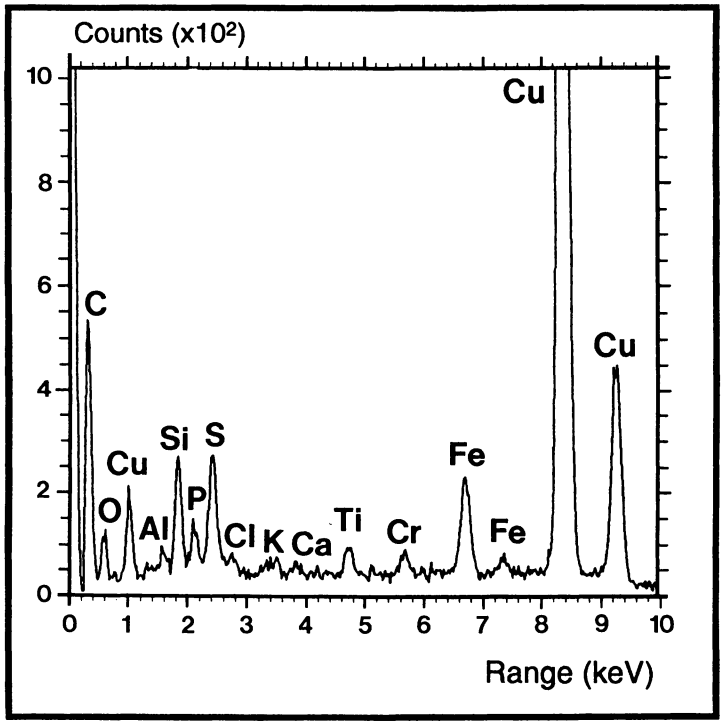

Figure 6. EDS spectra of metals complexed to "dissolved" organic material. Cu peaks are from the supporting grid and Cl peak is due to contamination from EPON.

In recent years, it has become increasingly apparent that consequential interactions exist between dissolved organic matter and the inorganic materials of freshwater systems. Studies have shown that significant quantities of trace metals are bound on the anionic surfaces of particulate humic substances (*65*). Constituent carboxyl and phenolic hydroxyl groups interact electrostatically with available cations in solution (*66*), forming organo-metallic complexes through ion exchange, surface adsorption, and chelation, with stabilities much higher than those of corresponding inorganic metal complexes (*63*).

Generally the concentration of dissolved solutes in a river system (approximately 30 mg/L, (*67*)) are more abundant than dissolved organic carbon (0.1 to 10 mg/L, with the upper value restricted to polluted systems (*68*). Under conditions of low DOC, interactions with metallic ions may cause only slight changes in the overall chemical composition of river water (*66*). Further, a majority of the reactive sites would be occupied by strongly bound metals such as Fe^{+3} or Al^{+3}, such that complexation of trace metals would be insignificant (*63*). It would, therefore, be advantageous to study a river system in which the relative abundance of dissolved organics to dissolved solutes would be much greater.

In the Amazon Basin, many of the rivers (blackwater varieties) are characterized by their high organic content and their solute-deficiency; the most notable being the Rio Negro with a TDS (total dissolved inorganic solids) of only 3.5 mg/L (*25*). The Rio Negro is the largest contributor of DOC to the Amazon River, whose average concentrations of 10.8 mg C/L greatly exceed those of the Rio Solimões with only 3.8 mg C/L (*7*). The Rio Negro is the major humic acid flux to the Amazon River system at 2.5 times the input of the Rio Solimões and also the largest fulvic acid flux amounting to 70% of the mainstream concentration. With a DOC:TDS of 3.1, the Rio Negro was chosen as an ideal study site for the role of dissolved organic matter in the complexation of dissolved metals. As the major tributary of the Amazon, which represents anywhere from 5 to 25% of the Amazon's discharge (*7*), any significant processes of metal cycling will have a marked influence on regional fluvial processes.

Samples of water were collected upstream of Manaus on the Rio Negro to identify DOC and determine its inorganic composition. Whole mounts of unfixed organic material (DOC) were prepared for electron microscopy by pipetting ~ 10 ❍L of water sample onto Formvar and carbon-coated copper grids. After allowing the water to evaporate off, the grids were analyzed by TEM and EDS.

Results from EDS analyses clearly revealed the reactive nature of the dissolved organic matter (Figure 6). Major cations in the waters of the Rio Negro, such as Fe, Si, and Al were shown to form the greater part of the organo-metallic complexes; contributing largely to the mobilization and transport of these metals in the river (*66*). The high organic-inorganic matter ratio of the river also seems to have provided sufficient reactive sites for the adsorption of Ca, K, P, and Mg, as well as trace metals, such as Ni, Cr, and Ti. Also, typical studies of dissolved metal concentration involve passing the water samples through 0.45 μm filters to remove suspended materials. Our results, however, indicated that many of the metals

which presumably occurred in "solution" may exist as colloidal metal-organic complexes (*66*).

As a whole, this process has profound implications for metal cycling in rivers which drain highly leached and low relief, podsolitic terrains. The interaction between dissolved organics and dissolved solutes may, however, be limited in other Amazonian river systems. In the Rio Negro, where suspended solids are found in extremely low concentrations, the humic substances behave rather conservatively with a HA:FA of 0.64. However, in the Amazon mainstream, the hydrophobic humic acids become selectively adsorbed onto fine suspended particles from the Rio Solimões (*6*), such that the HA:FA drops to only 0.31 (*7*). Although the fulvic acids are compositionally hydrophilic, and therefore, are not readily adsorbed onto detrital material, the drastic loss of humic acids could result in a decrease in available reactive sites for organo-metallic interactions.

Carbon-Isotope Studies in the Amazon Basin: Towards a Tool for Paleovegetation

Despite the fact that the Amazon Basin represents the largest contiguous area of tropical forest in the world, there remains no consensus as to the extent of closed forest cover in the Basin in the past (*69*). This represents a major gap in our understanding of the glacial-interglacial changes in terrestrial carbon storage (e.g., Crowley, (*70*)). The existence of "centres of endemism" within the Basin has led some workers to propose that the forest contracted to isolated "refugia" during cool, dry glacial periods and expanded across much of the Basin (as today) during warm, humid interglacial periods (e.g., Bigarella and Andrade-Lima, (*71*)). This hypothesis is supported by some palynological records from the eastern (*72*) and southeastern (*73*) basin, which show that grasslands existed during the last glacial period in the now forested regions surrounding the core sites.

The refugial hypothesis has been challenged by palynological records from the western Amazon Basin which reveal an uninterrupted dominance of forest biota, and also by new hypotheses which favor the maintenance of a high degree of endemism by hydraulic disturbance of the floodplain (*74,75*). Nelson et al. (*76*) have also demonstrated that some centres of endemism are an artifact of specimen collection densities.

The major barrier to producing a consistent record of vegetation change has been that many proxy vegetation and climate records yield only fragmentary information which is poorly time constrained, and which pertains only to a localized region. The carbon-isotope composition of organic matter preserved in ancient sediments offers the possibility of investigating past vegetation changes on a basin-wide scale. This is because closed forests are almost exclusively dominated by plants which photosynthesize via the C_3 photosynthetic pathway, with $\delta^{13}C$ values of ~-28‰. In contrast, tropical grasses which are common in open grassland/woodland (cerrado) areas, photosynthesize via the C_4 pathway, with

$\delta^{13}C$ values of ~-12‰ (*77*). Therefore, the $\delta^{13}C$ values of organic matter in river sediments will depend (among other things) upon the proportion of forest (C_3-) and grassland (C_4-) - derived carbon contributing to the carbon pool. A full discussion of the factors controlling the carbon-isotope composition of organic matter in fluvial sediments is provided by Bird et al. (*78*).

Terrestrial Sediments. In order to determine the range of values likely to be encountered in rivers with forested and non-forested catchments, suspended sediment and bottom sediment samples were collected and analyzed from the Tocantins/Araguaia River system, on the eastern margin of the Basin (*78*). This is the only major tributary of the Amazon River with a catchment that is not predominantly forested, and one of the few tributaries for which there is not already a substantial $\delta^{13}C$ database (*5,79*). In addition, rivers in the States of Rondonia and Acre, with catchments partly deforested (in the last twenty years) were also sampled to determine how rapidly changes in the catchment vegetation are registered in the $\delta^{13}C$ value of riverine POC.

Figure 7 shows that there is a difference of 2-4‰ between the $\delta^{13}C$ values of organic matter from rivers draining forest versus cerrado catchments during the wet season, but no difference during the dry season. The lack of difference in the dry season implies that most rivers in the cerrado region are fringed by a C_3-dominated strip of forest, which provides the bulk of the carbon exported during the dry season (-27 to -30‰). During the wet season, high runoff rates transport C_4 carbon to the river from more remote areas leading to $\delta^{13}C$ values as high as -24.6‰.

The $\delta^{13}C$ value of the POC is rivers draining forested catchments is the same as that of the forest vegetation during both the wet and dry seasons. However, in rivers draining cerrado catchments, the $\delta^{13}C$ values of POC are consistently lower than in the bulk vegetation (cerrado soils have $\delta^{13}C$ values between -15 and -25‰). This is due to the afore-mentioned bias toward C_3 carbon derived from close to the river, possible preferential metabolism of C_4 carbon by micro-organisms in the river, and some contribution from low-$\delta^{13}C$ algal biomass (*78*).

The $\delta^{13}C$ values of the POC in rivers draining deforested catchments span almost the entire range of values found in the forested and non-forested catchments (-23.5 to -29.7‰), with the coarse (>63 μm) fractions of the samples tending to be 1-2‰ enriched in ^{13}C compared with the fine (<63 μm) fraction.

The results from the study suggest that, while the $\delta^{13}C$ value of POC from rivers draining non-forested catchments does not accurately reflect the bulk $\delta^{13}C$ value of biomass in the catchment, the non-forest $\delta^{13}C$ signature can nonetheless be readily distinguished from the $\delta^{13}C$ signature of POC in rivers draining forested catchments. These findings are in accord with data from the Zaire (*80*) and Sanaga (*81*) River systems in Africa, where $\delta^{13}C$ values from -14.6‰ have been recorded from rivers draining non-forested catchments. The isotopic composition of POC from rivers with deforested catchments in the Amazon Basin suggests that the $\delta^{13}C$ value of coarse POC responds to changes in catchment

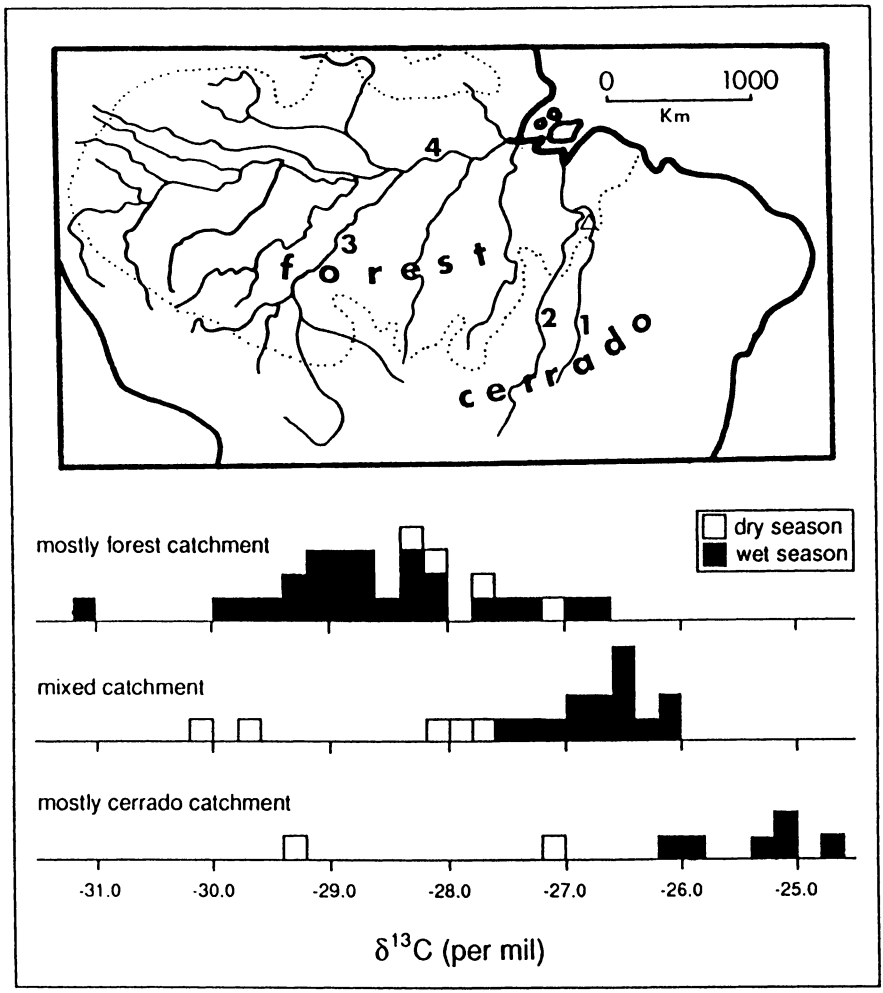

Figure 7. Carbon isotope results for POC from rivers in the Amazon Basin [additional data from Hedges et al. (*5*) and Cai et al. (*79*)]. 1. Tocantins R.; 2. Araguaia R.; 3. Madeira R., 4. Amazon R. Dotted line indicates present extent of forest. General regions in which samples were collected for this study indicated by letters: (A) Marabá-Tocantinopolis, Pará; (B) Carajás, Pará; (C) Ariquemes, Rondonia; (D) Rio Branco, Acre. $\delta^{13}C$ results reported in per mil, relative to the PDB standard (from Bird et al. (*78*)).

vegetation on timescales of years to decades, while that of fine POC may take longer to respond.

Biomarker Carbon-Isotope Analyses. While a forest/non-forest carbon-isotope signature is readily identifiable in terrestrial environments, it is very difficult to obtain complete, well dated fluvial sequences. Complete sedimentary sequences are readily available from the submarine fan deposits which lie off the mouth of the Amazon River (*82*), but the analysis of bulk sediments from the marine environment is not appropriate because terrestrially-derived riverborne carbon in the sample rapidly becomes mixed with marine-derived carbon offshore from the river mouth.

One way of circumventing these problems is to utilize biomarker compounds for isotopic analysis which are specific to terrestrial vegetation. There are many such compounds, and two classes which offer considerable potential are the long-chain n-alkanes and the lignin-derived phenols.

N-alkanes. Straight chain hydrocarbons (n-alkanes) are common minor components of algae, bacteria and vascular plants (*83*), and are comparatively resistant to diagenetic alteration (*84*). Algae and bacteria are generally characterized by n-alkane predominances at low carbon numbers (C_{16}-C_{24}), usually with little difference in the relative abundance of n-alkanes with odd or even carbon numbers (low carbon preference index - CPI). In contrast, vascular plants are characterized by peak n-alkane abundances at high carbon numbers (C_{27}-C_{33}), with a strong preference for odd over even carbon numbers (high CPI's) (*83*).

Gas-chromatography-combustion-mass-spectrometry (GC-C-MS) enables the carbon-isotope analysis of n-alkanes of each carbon number, and therefore, the separate analysis of alkanes derived from algal/bacterial and vascular plant sources. This ability has previously been utilized to determine the origin of waxy n-alkanes in a variety of sediments (*85,86*). The carbon-isotope composition of n-alkanes derived from vascular plants can, therefore, be used to determine the relative contributions of C_3- and C_4-derived carbon to organic matter in marine, terrestrial or composite sediment samples. This approach has been applied in a preliminary manner to representative samples from the Amazon Basin (Bird and Summons, unpublished data).

The river sediment samples (RIV-NF, catchment not forested, i.e. woodland/grassland dominated; RIV-F, catchment forested) both show strong modes at C_{29}- C_{31} with high CPI values (Figure 8A) consistent with organic matter in the samples being derived predominantly from vascular plant sources. In addition, both samples contain shorter chain n-alkanes (down to C_{15}), suggestive of an algal/bacterial contribution to the bulk carbon in the samples.

The marine samples (MAR-P, proximal marine, close to the river mouth; MAR-D distal marine) have bimodal n-alkane distributions (Figure 8B), with peaks at C_{29}-C_{31}, from terrestrial carbon discharged by the Amazon River, and broader

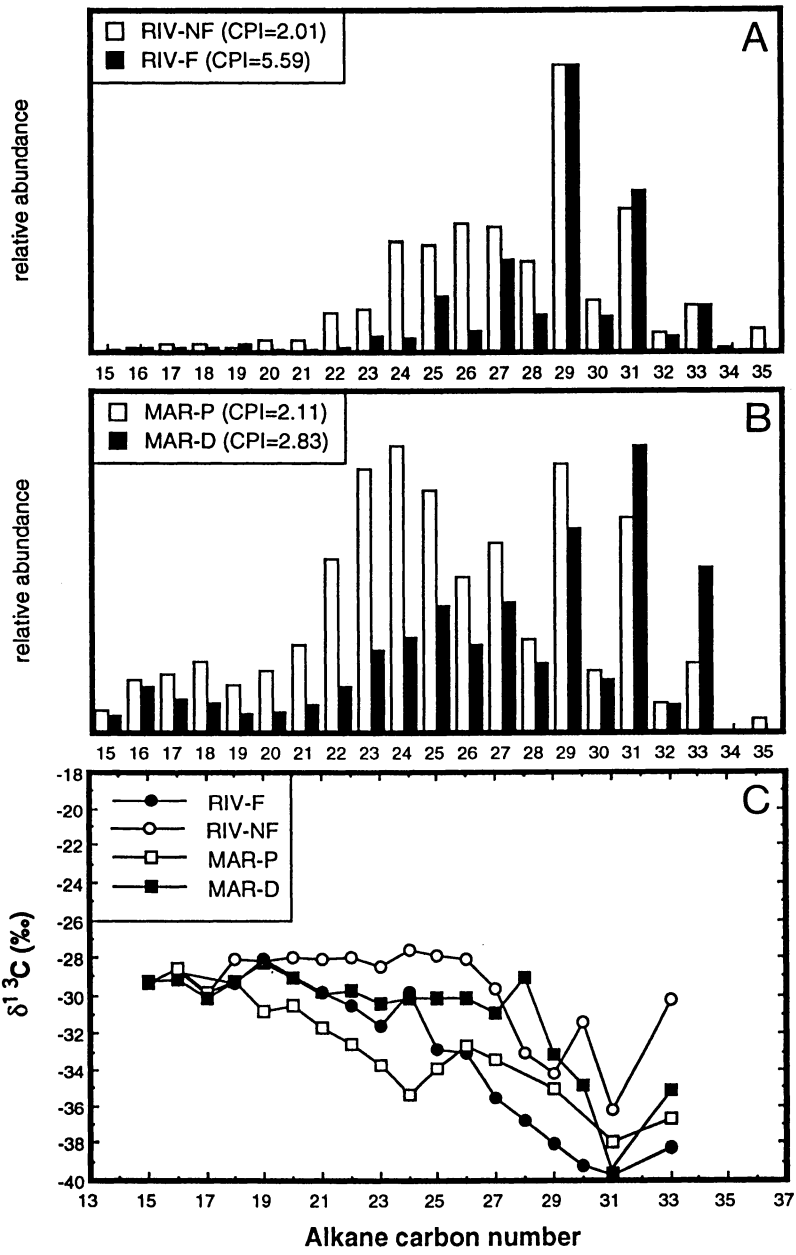

Figure 8. Relative abundances of n-alkanes in sediments from (a) forested-F and non-forested-NF rivers in the Amazon Basin and (b) distal-D and proximal-P marine sediments off the mouth of the Amazon River. $\delta^{13}C$ values for individual n-alkanes in both riverine and marine samples is given in (c), relative to the PDB standard (from Bird et al., in prep.).

peaks around C_{24} due to algal/bacterial input from the marine environment. The shape of the mode at around C_{24}, in both samples, suggests that n-alkanes derived from algae/bacteria probably contributes significantly to the predominantly terrestrial C_{27} peak and possibly a small amount to the C_{29} peak. In both the river and marine sediments, there is a strong preference for odd over even carbon numbers at high carbon numbers, which become progressively weaker below ~C_{25}.

The $\delta^{13}C$ values for n-alkanes from river and marine sediment samples are shown in Figure 8C. They exhibit approximately constant values between -28 and -30‰ at low carbon number, consistent with a mixed algal/bacterial source, decreasing to variably lower values with increasing carbon number. The $\delta^{13}C$ values for n-alkanes from RIV-NF (non-forested catchment) are consistently higher than for the same n-alkane in RIV-F (forested catchment), as expected from the bulk $\delta^{13}C$ values of the samples, and consistent with the higher proportion of C_4 biomass in the non-forested catchment.

The marine sediment samples have n-alkane $\delta^{13}C$ values which are slightly higher than the sample from the forested catchment (RIV-F) at high carbon numbers, tending to progressively higher values at lower carbon numbers. The amount-weighted mean $\delta^{13}C$ value of the odd-numbered n-alkanes at carbon numbers of 29 or higher (terrestrially-derived) in both the marine samples are intermediate between the corresponding values for the river samples. This is to be expected, as the carbon currently exported from the Amazon Basin is derived from a mix of forested and non-forested sources. Sample MAR-P exhibits comparatively low $\delta^{13}C$ values at carbon numbers between C_{19} and C_{25}, with a pronounced minimum at C_{24}, corresponding to the lower carbon number peak in n-alkane abundance in the sample. It is possible that these low values result from a comparatively large bacterial hydrocarbon component in this sample.

The results discussed above should be considered preliminary, but they do suggest that the carbon-isotope composition of terrestrially derived n-alkanes accurately reflect the isotopic composition of the bulk vegetation from which they were derived. They also suggest that this terrestrial isotopic signature can be resolved in marine sediments, where the bulk terrestrial carbon-isotope signature is obscured by admixture with marine-derived carbon.

Lignin-derived phenols. Lignin compounds are phenolic polymers that form a major component of the cell walls of vascular plants. They are comparatively resistant to degradation, and are common constituents of soil and sediments, including those of the Amazon Basin.

Upon oxidative degradation, the complex lignin polymers break down into a suite of simple lignin-derived phenols which are indicative of their source. Of these, p-coumaric acid occurs only in non-woody angiosperm and gymnosperm tissues (*87*), and is therefore, of considerable interest as a potential carrier of a carbon isotope signal for C_3/C_4 ratios in the catchment vegetation. Both

compounds have been identified as constituents of terrestrial and marine sediments (*5,88*).

Preliminary results have been obtained for both p-coumaric acid extracted from plant samples using a 1N NaOH extraction under nitrogen, followed by separation of the phenolic component by either extraction and isolation of the individual lignin-derived phenols using reversed-phase preparative-scale HPLC (e.g., Hartley and Buchan (*89*)). The results, detailed in Table IV, are consistent with previous findings that the bulk "lignin" component of plants is depleted in ^{13}C relative to the bulk plant tissue by 2-7‰ (*90*). Comparison of the results for p-coumaric acid with the bulk lignin-derived phenol fraction suggests that p-coumaric acid may be less depleted in ^{13}C than bulk lignin.

Table IV. Carbon-Isotope Composition of Bulk Vegetation, Bulk Lignin-Derived Phenol (LDP) Fraction and Isolated p-Coumaric Acid (PCA)

Sample	$\delta^{13}C$ *bulk*	$\delta^{13}C_{LDP}$ *bulk*	$\delta^{13}C_{PCA}$ *1st extinction*	$\delta^{13}C_{PCA}$ *2nd extraction*
Corn Cob (C4)	-12.1	n.d.	-15.4	-15.8
Sugar Cane Stalk (C4)	-12.8	-15.4	-15.2	n.d.
Bamboo Stalk (C3)	-27.8	-31.2	-30.3	-30.7
Wheat Stalk (C3)	-25.5	n.d.	-28.3	-29.3

Chemical Evidence in the Acre Subbasin for Arid Climate Conditions During the Last Glacial Cycle. The Acre subbasin of western Amazonia contains mainly fine-grained sediments (representing a fluvial-lacustrine system) with veins of calcium sulfate (gypsum) and calcium carbonate (aragonite) concretions. The presence of these precipitates is considered strong supporting evidence for arid conditions. Radiocarbon ages of carbonate samples, ranging up to 53,000 yr BP, indicate arid climate conditions during the Last Glacial Cycle. The preservation of these older sediments on the surface is attributed to the lack of contemporary input of Andean sediments. This is due to the separation of rivers in the Acre region from adjacent upper Andean tributaries by a small mountain range (Serra do Divisor) along the contemporary Peruvian/Brazilian border. Thus, the modern rivers flowing through the Acre region comprise of reworked sediments, deposited prior to the formation of the Serra do Divisor. Satellite imagery revealed the original system as a mega alluvial fan extending from the Andean highlands to the Acre region (~1,000,000 km^2), with the Acre subbasin representing the distal portion of the original fan system. (*91*).

Deciphering Chemical Signatures on Amazonian Surface Materials

Chemical weathering refers to the dissolution of rocks by surface waters. Rocks are physical mixtures of silicate minerals, characterized by their symmetrical arrangements of silicon and oxygen. Aluminum, Ca, Mg, Na and K are also present in surface rocks at per cent levels. Chemical weathering of continental rocks may

be modelled in terms of feldspar dissolution, the most abundant minerals in the earth's crust (*92*):

$$3H_2O + 2KAlSi_3O_8 \rightarrow Al_2Si_2O_5(OH)_4 + 4SiO_2 + 2K^+ + 2OH^- \quad (1)$$
(aq) K-feldspar(s) kaolinite (s) (aq) (aq) (aq)

$$H_2O + Al_2Si_2O_5(OH)_4 \rightarrow 2Al(OH)_3 + 2SiO_2 \quad (2)$$
(aq) kaolinite (s) gibbsite(s) (aq)

These reactions are chemically driven by the high degree of disequilibrium of the "feldspar-rainwater" system. Feldspars crystallize from molten magmas at ~1000°C and thus are not in equilibrium with earth surface conditions. On a global scale the influence of chemical weathering is reflected in the differences in concentration of rock-derived solutes between average rain water and average river water (Table V a). The incongruent dissolution of primary rock minerals, such as feldspars, is accompanied by the formation of secondary minerals, typically clay mineral groups. The fundamental difference between primary aluminosilicate-silicate minerals and clay minerals is the degree of long-range order: the former having strong chemical bonds in three directions, while in clay minerals, strong bonds between the major components (O, Al, Si) exist in only two directions. The variations in spacing between weakly bonded layers is typically used to characterize clay mineralogy.

Table V(a). Compositions of surface waters (in μg/ml)

	World Average		*Central Amazonia*	
	[1]Rain	[2]Rain	[3]Rain	[3]Rivers
Na	2.0	6.0	0.007	0.2-2
SiO_2	<0.01	13.0	<0.01	3.0-12.0
K	0.3	2.0	0.008	0.2-2.0
Ca	0.09	15.0	0.004	0.2-2.0

Note: values from [1]Garrels and Mackenzie (*93*), [2]Livingston (*94*), and [3]Stallard and Edmond (*13*).

In our approach, three types of minerals accumulate as weathering proceeds and serve as indicators of regional chemical weathering intensity:

1. Complex clay minerals incorporate cations (Na^+, K^+, Mg^{2+}, Ca^{2+}) into their lattices and have high capacities to exchange these ions (mainly for H^+ ions). Their lattices also have significant hydration capacities by incorporating hydroxyl ions.
2. In kaolin group minerals, aluminosilicate sheets are more closely spaced than in complex clays. Due to fewer interstitial and surface sites for incorporating and exchanging major element cations (Na^+, K^+, Mg^{2+}, Ca^{2+}) their compositions are expressed as ratios of Al, Si, O and OH.

3. Aluminum oxide/hydroxide phases, such as gibbsite [$Al(OH)_3$], accumulate from the dissolution of kaolin phases [equation (2)] during the final stages of weathering.

It is important to note that any of these mineral phases may form transiently (as weathering proceeds) depending on local pore and ground water salinities.

During the initial and intermediate stages of weathering, the formation of complex clay minerals is sustained by high salinity surface waters that are in contact with the primary rock minerals (Figure 9, dashed line). This situation is prevalent in much of the northern hemisphere where continental-scale glacial advances (over the past two million years) renewed land surfaces with abundant fresh rock debris. Depending on regional rainfall and the extent of mineral surfaces available for reaction, these conditions may prevail for thousands of years or until weathering profiles are deep enough to remove surface waters from contact with primary rock minerals. At this stage the diminished salinities in pore waters in the weather cover favour the formation of kaolin phases. The dominance of kaolinite throughout much of lower Amazonia suggests that this region is at an advanced stage of weathering (Figure 9), with weathering profiles often exceeding 100m.

In general, the gradual mineralogical and chemical changes that arise in surface soil and sediment as weathering proceeds, is reflected by the chemical composition of regional river systems. For example, the rivers draining the highly weathered Amazonian lowlands have significantly lower rock-derived constituents than the mountainous Andean tributaries (Table V b). Data from central Amazonian rivers show higher silica/cation ratios than in average river water, indicating these waters are in contact with materials in transition from advanced to extreme weathering stages (Table V a). Kaolin phases are buffered by high levels of silica (e.g., 10 Ωg/ml), derived mainly from feldspars in the initial and intermediate stages of weathering, and from quartz during advanced to extreme weathering. That feldspar dissolution is virtually complete in central Amazonia, is indicated by the low levels of the major cations in feldspars (Na, K and Ca). In these rainforested areas there is evidence that biological particulates are the main sources of Na, K and Ca ions (*13,96*).

Table V(b). Salinity data for Amazonian River waters (in Ωg/ml)

Drainage Basin	*Dry Season*	*Wet Season*
Mountainous Andean Streams	36-248	84-144
Tributaries draining both highlands and lowlands	17-84	8-50
Central Amazonia	5-51	4-22
Amazon River mouth	48	28

Values taken from Kronberg et al. (*97*) and Gibbs (*28*).

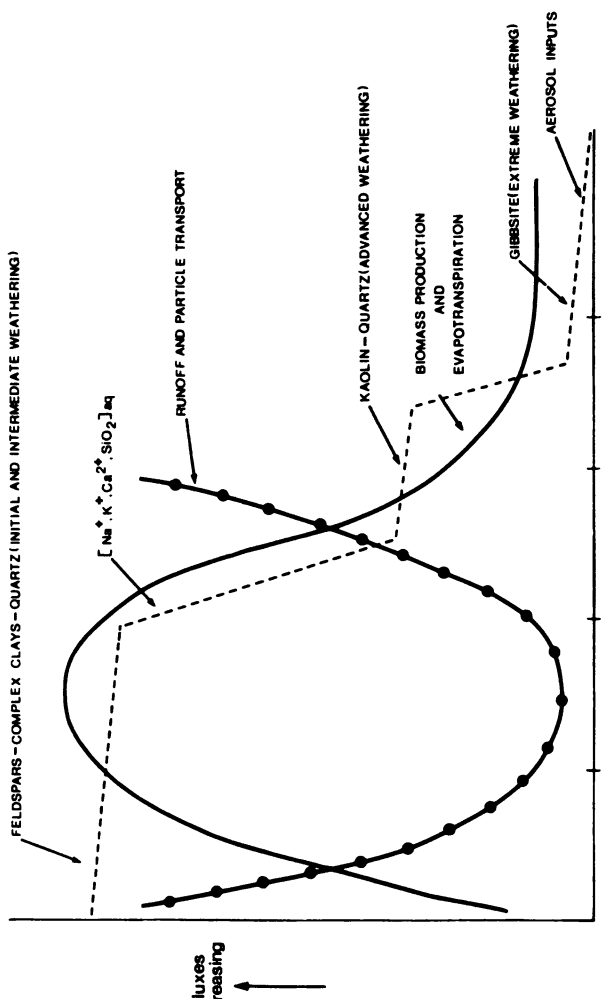

Figure 9. Interplay of variables during weathering. (1) In intensely weathered rainforested regions evapotranspiration is maintained although there is no net biomass productivity. (2) As weathering intensifies, soil nutrient reserves become depleted and in the normal course of events, both net biomass productivity and evapotranspiration fall (from Kronberg et al. (95)).

In eastern Amazonia massive Al accumulations (the Paragominas and Trombetas bauxite deposits) provide evidence that the erosional regime in these areas are extremely weathered. Such intense weathering requires extensive water/mineral interaction over long periods of time. Aluminum accumulation may be facilitated by increasing porosities (if low overburden pressures are maintained as weathering proceeds) due to decreases in molar volumes of up to 70 % in aluminum hydroxide phases relative to complex clay minerals. Isotope studies of gibbsite phases from the Paragominas area (*98*) indicate extremely low ^{18}O values (-9‰) relative to the modern ^{18}O values of the Carajás region samples. This implies that the formation of aluminum oxide phases occurred in the former area during a strongly monsoonal climate regime. $^{40}Ar/^{39}Ar$ dating of K-bearing manganese from the Carajás region further suggests a complex weathering history dating from the mid-Tertiary (~30 million years ago). Therefore, the massive bauxite deposits to the north and east of Carajás likely formed earlier. It is then possible that weathering over tens of millions of years were required to produce the quasi continuous layers of bauxite extending over ~100,000 ha at the Paragominas deposit (*99*).

Weathering Time Constants and Geological Constraints. A minimum rate of chemical weathering can be ascertained by estimating the time required for the dissolution of 1 m of continental crust (density, 2g/cm^3) that receives 1 m rainfall per year, with rock mineral constituents removed in solution at levels found in average river water (~100 ug/ml). Under these conditions, continental surfaces would be lowered by 1m every 20,000 yr (50 m/million years). This figure falls within the range (10-100 m/million years) of other estimates of continental erosion (*100*).

Consideration of these time constants and the average elevation above sea level (500 m) of continental crust underscores the importance of both geologically constructive processes, such as volcanic activity, which adds ~ 1 billion tons of new rock material to continental surfaces every year, or major episodic glacial events. Therefore, the degree of advanced weathering found in lower Amazonia indicates that this region was both isolated (for tens of millions of years) from constructive geological processes (i.e. by being remote from tectonic plate margins) and was located within humid, tropical latitudes.

Chemical Trends During Weathering. As chemical weathering progresses there is an overall transfer of rock mineral constituents to the hydrosphere. In the initial and intermediate stages of weathering elements may be transiently stored in complex clay phases, until weathering depths prevent surface waters from maintaining contact with primary minerals. Hence, chemical compositions of young soils are typically similar to those of surface rocks (Table VI), however, with different mineral assemblages. As weathering advances and kaolin phases accumulate, levels of most major elements diminish substantially (see Amazonian soils, Table VI) relative to crustal abundances. Data for 30-40 minor and trace elements obtained using spark source mass spectrometry showed that as weathering intensifies some elements (e.g., Cl, As, Sb, Sn, I, Cs, Pb) became enriched relative to their crustal abundances, whereby most others became

depleted. Elements with the most strongly depleted concentrations included the alkali metals (except Cs), the alkaline earths and most first row transition metals. Elements displaying enrichment may participate in sorption processes. For example, laboratory studies showed that iodine could be strongly sorbed onto iron hydroxide surfaces. Some refractory elements, such as Ti and Zr, considered to have relatively immobile oxide phases, exhibited depletion with depth in some bauxite profiles. Concentration trends among minor and trace elements during weathering cannot be readily explained in terms of their physico-chemical properties in bulk phases. Their chemical pathways during weathering appear to involve an array of processes including, formation of complex ions, surface reactions, dissolution and reprecipitation, as well as processes that may be mediated by the microbiosphere (*99,100*).

Table VI. Compositions of Rocks and Weathered Materials (in wt%)

	[1]*Surface Rocks*	[2]*Young Soils*	[3]*Amazonian Soils (Lower Basin)*	[4]*Amazonian Bauxite (Paragominas)*	*Andean-Derived Sediments*
Na	3.0	0.5	0.03	0.002-0.006	0.3
Al	9.0	5.3	11.0	20.0-32.0	10.0
Si	31.0	28.0	13.0	1.0-5.0	27.0
K	3.0	2.0	0.2	0.002-0.02	2.2
Ca	3.0	2.0	0.005	0.0002-0.0005	0.3
	f,qz	qz,f,cl,ca	ko,qz,go	gi,hte,ko	qz,ko,il

Values from [1]Taylor and MacLennan (*24*), [2]Kronberg (unpub. data), [3]Kronberg et al. (*99*), [4]Kronberg et al. (*100*), and [5]Kronberg et al. (*97*).
f=feldspar, qz=quartz, cl=chlorite, ca=calcite, ko=kaolinite, go=goethite, hte=hematite, il=ilmenite

Iron also accumulates during extreme weathering processes. The original source of iron is from silicate minerals, such as pyroxene and amphibole minerals, while in highly weathered terrains Fe appears mainly as oxides, with highly variable degrees of crystallinity, colours, morphologies and levels of aggregation.

Weathering and Soil Fertility. The general infertility of soils in the lower Amazonian Basin is shown by the depletion (often by 1 or 2 orders of magnitude relative to young soils) of major rock-derived nutrients such as K, Ca, Mg and most first row transition elements. In the past, the vast rainforests covering much of the lower Basin have raised hopes of agricultural potential in Amazonia. However, considering the Ca value (0.005%, Table VI) for a typical Amazonian soil (density 2.0 g/cm^3), the growing layer (upper 10 cm) of 1 ha of such land would merely contain 100 kg total of Ca. This compares to 40,000 kg in young soils (Table VI). Given that a typical grain crop will remove 20-40 kg of Ca in the harvested biomass, only 1-2 harvests could be theoretically possible. In addition, at

these concentration levels (50 uOg/g) laboratory experiments have shown that Ca is not exchangeable. The infertility of these soils becomes abundantly clear when similar depletion levels are extended to the 20-30 other bioessential elements (*99*).

The explanation for extensive Amazonian rainforests overlying infertile soils is their capacity to store and recycle nutrients within the biomass. Stark and Jordan (*101*) have shown that nutrient losses to ground and stream waters are balanced by rain and aerosol additions. Some atmospheric inputs are derived from as far away as the Sahara, estimated to supply Amazonia with ~1 kg P/ha/yr. The Amazonian forests also participate in regional and global water and energy cycles by virtue of the large quantities of latent heat transferred to the atmosphere as water is vaporized from leaf surfaces (*102*). Tropical regions, such as Amazonia, also provide much of the sensible heat (i.e. heat exchanged as air passes over the Earth's surface) that is transported poleward and contributes to balancing negative radiation losses at higher latitudes (*103*).

Weathering of Mineral Deposits

Over the past decade there has been great interest in the weathering of ores and areas of metal enrichment, particularly in the Carajás region of the Amazon. The Carajás region is located in an Archean continental rift basin, where the late Archean and early Proterozoic rift-filling sequences are represented by metavolcanic and metasedimentary rocks. These rocks contain the world's largest high-grade iron deposits, together with significant resources of Cu, Mn, Au, Ag and Cr. Intense chemical weathering of these rocks (or deposits) resulted in further enrichment of metals near the surface in the form of lateritic deposits (*104*), with accumulation of Fe-oxides (mainly goethite and hematite), Mn-oxides (mainly cryptomelane, hollandite and lithiophorite) and kaolinite.

The Igarapé Bahia lateritic gold deposit is located in northwest part of the Carajás plateau at an elevation of 650 m. This plateau is incised to elevations of 400 m by the steep-sided valley of Igarapé (stream) Bahia and several small tributary streams (Figure 10). Due to the strong weathering over millions of years, and the resultant formation of advanced laterite profiles, this region provided a unique opportunity to study the geochemical behavior of various elements during laterisation.

Laterite Profiles. The laterite profiles can be divided into six horizons (*105,106*). From unweathered bedrock to top, the profiles comprise of a saprolite zone, pallid zone, mottled zone, ferruginous zone and topsoil (Figure 11). The unweathered bedrock is mainly composed of quartz and chlorite, with sulfide-quartz veinlets and impregnated sulfide minerals (mainly chalcopyrite and bornite). Other minerals, as identified by electron microprobe, include calcite, albite, micas, and accessory minerals. The saprolite is as much as 40 m thick, consisting of clay minerals, Fe-oxides, Mn-oxides and some relict primary minerals. The pallid zone is as much as 20 m thick and is characterized by pure white to multicolored kaolinitic clays with quartz, ilmenite and goethite. The mottled zone is as much as 100 m thick, and is composed of yellow to brown kaolinitic clays with mottled and blocky ferruginous

lumps. Lastly, the ferruginous zone is as much as 25 m thick, and is dominated by Fe-oxide nodules and Mn-oxides in the lower level, with small amounts of kaolinite, quartz and gibbsite.

Laterite formation is attributed to continuous leaching of alkalis, alkaline earths, and some SiO_2 (*105-109*). A mottled zone is developed by local redistribution of Fe, which overlies the saprolite above the water table level. As weathering proceeds Al and Si are progressively removed from the upper part of the profile whereas Fe-oxides are retained to form a ferruginous zone. At Igarapé Bahia, however, the profile is characterized by a major pallid zone, suggesting that this profile presumably developed through two main stages: (1) development of the ferruginous zone and mottled zone with saprolite over the unweathered rocks, and (2) incision of landscape and modification of the profile to form the pallid zone and more saprolite.

Major-Oxide Geochemistry. The major-oxide data of bedrock and laterite samples were analyzed by X-ray fluorescence spectrometry (XRF), and are presented in Table VII. In the profiles, from base to top, Fe_2O_3 increases, whereas in the pallid zone it becomes depleted relative to the other weathered zones. The SiO_2 decreases from base to top. The Al_2O_3 increases from base to the mottled zone, where kaolinite is predominant, then decreases to the ferruginous zone. The MnO is enriched in the lower levels of the ferruginous zone. The TiO_2 is mainly enriched in the mottled zone as relict ilmenite. The P_2O_5 shows a progressive enrichment trend, due both to the sorption by goethite, the stability of phosphate minerals (monazite, churchite, apatite), and its biological affinity (*110*). Alkaline and alkaline earth oxides are depleted in most laterite samples with trace amounts of K_2O (in some samples) due to presence of cryptomelane. The MgO in upper

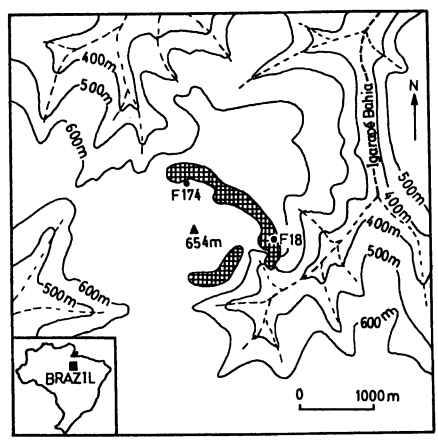

Figure 10. Topographic map of the Igarapé Bahia lateritic gold deposit, showing locations of boreholes F18 and F174. Test pit 12 is located 25m west of borehole F18. Shaded areas represent gold ore zones (from Zang and Fyfe (*105*)).

levels are mainly attributed to relict tourmaline. Na_2O values are commonly below the detection limit for XRF.

Trace-Element Geochemistry. Trace element concentration in the profile are given in Table VIII. The Euclidean distances between elements are rescaled and plotted in a dendrogram (Figure 12) that revealed four distinct element associations, namely Fe-, Mn-, Al- and Si-correlated elements.

Fe-Correlated Elements. This association includes Fe, P, Nb, Au, Ag, Sr, Y, La, Ce, Pb, Pt. Pd and Mo. These elements are characterized by process enrichment, with an increasing trend from base to top of profile. They are also enriched in the Fe-rich breccia zone, reflecting their associations with Fe-oxides. Palladium and Pt, which are not included in the cluster analysis, also show a similar enrichment pattern as Fe, suggesting that they may also belong to this association. Two Ag-Pd alloy grains were identified in the ferruginous zone (*111*).

Immobility of Nb has also been documented in other laterite profiles (*100,112,113*). The correlation of Nb with Ti and Fe suggests that Nb is hosted by relict rutile and Fe-oxides. Molybdenum and Pb are probably adsorbed by goethite (*114*), whereas the accumulation of phosphate minerals in the ferruginous zone leads to the enrichment of Y and some light rare earth elements (La, Ce). However, the positive Ce anomaly is mainly due to formation of cerianite (CeO_2) in laterite (*106*).

Native gold and electrum (Ag-Au alloy) are found within Fe-oxide nodules in the ferruginous zone. Most of the gold grains are less than 10 microns in size. The fineness [1000xAu/(Au+Ag)] of gold increases downwards in the profile, suggesting a three-stage genetic model for the lateritic deposit (*105*). In the first stage thiosulfate ions from weathering of sulfides are believed to transport both Au and Ag into the profiles to form the electrum. In the second stage, both Au and Ag are then remobilized and incorporated into the ferruginous zone as the erosion surface was lowered by weathering. In the third stage, after uplift and incision of the landscape, chloride leaching separated Ag from the gold grains to purify the electrum. The survival of electrum in the top of the profile can be attributed to lower chloride concentrations and enrichment of organic matter in the near-surface environment.

Mn-Correlated Elements. This association includes most of the first-row transition metals (Sc, Mn, Co, Ni, Cu, Zn), as well as Ba and Cd. These elements are characterized by an enrichment in the lower level of the ferruginous zone and the upper level of the mottled zone. They are enriched in either Mn-oxides or Fe-oxides. Ba (in the form of hollandite) comprises up to 4.93 wt%. Concentrations of trace elements in goethite decrease from the base to the top in the profile, due to increase of crystallinity of goethite or reworking of the mineral (*106*). Thus some trace elements follow the pattern of Mn enrichment although they may be enriched in goethite.

Publication Date: March 31, 1995 | doi: 10.1021/bk-1995-0588.ch018

Table VII. Major-oxide compositions of the laterite profile (wt%)

Sample	*depth(m)*	Fe_2O_3	Al_2O_3	SiO_2	*MnO*	TiO_2	*MgO*	*CaO*	K_2O	P_2O_5	*LOI*	*total*
					ferruginous zone							
B95	0.0-2.0	74.83	5.87	3.27	2.21	0.03	-	-	0.02	0.55	12.10	98.88
F18-7	3.5-3.7	70.94	11.74	4.62	0.22	0.28	0.70	-	-	0.90	10.49	99.94
P-1	6.9-10.5	75.34	5.98	5.60	1.90	0.38	0.76	0.02	0.08	1.20	8.40	99.73
P-3	12.0-14.0	76.32	4.19	3.67	4.90	0.42	0.66	-	0.06	0.93	8.83	100.04
P-6	18.0-20.0	86.56	0.96	3.59	0.22	0.16	0.74	-	0.02	0.98	7.01	100.29
P-7	20.0-21.0	58.94	12.64	12.32	1.14	1.44	0.68	-	0.04	0.78	12.41	100.47
					mottled zone							
F18-16	24.7-25.0	44.52	20.28	21.81	0.21	1.68	0.36	-	-	0.53	10.44	99.87
F18-20	39.1-39.3	39.83	20.98	22.60	0.58	3.77	0.30	-	0.01	0.44	11.52	100.08
F18-27	70.2-70.4	39.22	22.53	25.04	0.66	1.30	0.33	-	-	0.28	10.55	99.94
F18-32	82.0-82.2	58.29	13.83	13.84	2.03	0.73	0.70	0.02	0.05	0.89	10.00	100.41
					pallid zone							
F18-41	118-119	20.35	22.85	42.35	0.44	4.10	0.22	-	0.02	0.13	9.65	100.15
					saprolite zone							
F18-50	148-162	4.77	13.88	47.54	0.14	0.92	8.60	0.23	0.01	0.19	5.52	100.01
					unweathered rock							
F18-55	217-226	4.74	5.03	86.12	0.03	0.11	1.36	0.06	0.84	0.06	1.32	99.73
F10	241.9	13.64	14.30	47.64	0.22	1.32	4.59	6.86	0.55	0.10	2.83	100.38
F14	261.6	14.09	13.76	52.06	0.15	1.47	6.52	3.09	0.51	0.20	4.18	100.08

Total Fe content as Fe_2O_3; LOI=loss on ignition. Na_2O is 3.49 and 2.58 in F10 and F14, respectively, and is lower than 0.01 in other samples. Values from Zang and Fyfe (*105*).

Seidl et al.; Chemistry of the Amazon
ACS Symposium Series; American Chemical Society: Washington, DC, 1995.

Table VIII. Trace-element concentrations in the laterite profile (ppm)

Sample	*Sr*	*Ba*	*Sc*	*V*	*Cr*	*Co*	*Ni*	*La*	*Ce*	*Y*	*Zr*	*Nb*	*Mo*
B95	11	461	23	218	<1	96	51	150	1321	30	15	18	139
F18-7	52	43	19	149	59	44	77	792	399	22	37	18	149
P-1	327	561	50	135	34	105	69	>2000	>2000	110	54	27	288
P-3	75	475	40	132	21	76	58	1262	>2000	78	55	32	245
P-6	10	27	14	70	70	34	77	417	379	24	26	26	110
P-7	23	148	47	153	63	32	65	987	>2000	33	181	37	173
F18-16	3	82	19	257	162	16	82	49	154	10	113	13	17
F18-20	8	458	67	358	24	27	32	51	67	23	277	21	9
F18-27	3	44	50	298	42	16	44	499	58	12	110	13	7
F18-32	59	734	68	245	45	106	158	307	324	44	81	16	76
F18-41	11	45	62	320	32	30	30	63	123	31	288	6	5
F18-50	2	7	20	133	157	45	117	45	60	13	117	14	4
F18-55	5	96	3	24	119	8	49	20	27	2	56	4	6
F10	53	71	26	236	107	35	42	16	21	8	59	12	3
F14	62	112	26	225	36	37	26	41	51	23	105	15	3

Sample	Ga	Cu	Pb	Zn	Cd	Ag	Au	Pt	Pd	S	Cl
B95	<2	6891	154	85	2	4.9	10.730	0.010	0.083	440	141
F18-7	<2	2006	62	17	3	3.9	1.930	<0.005	<0.001	210	126
P-1	<2	2867	160	17	3	25.0	2.860	<0.005	0.004	540	63
P-3	3	7080	136	16	2	22.1	0.314	<0.005	<0.001	640	90
P-6	<2	1913	112	29	2	40.3	11.160	<0.005	0.006	560	90
P-7	8	4997	116	26	2	11.5	6.980	<0.005	0.027	560	180
F18-16	15	946	11	14	1	<0.5	0.300	<0.005	<0.001	220	99
F18-20	33	2114	89	24	2	<0.5	0.070	<0.005	<0.001	220	216
F18-27	20	738	<2	9	2	<0.5	0.060	0.009	0.021	100	90
F18-32	9	5816	36	60	3	3.2	1.891	<0.005	<0.001	110	126
F18-41	39	368	6	53	2	<0.5	0.007	<0.005	<0.001	100	171
F18-50	17	145	2	45	<1	0.5	0.003	0.005	0.002	220	99
F18-55	14	1126	<2	13	<1	0.5	0.014	<0.005	<0.001	1340	135
F10	28	31	9	65	<1	0.7	<0.001	<0.005	<0.001	110	171
F14	30	170	40	40	<1	1.1	<0.001	<0.005	<0.001	1560	126

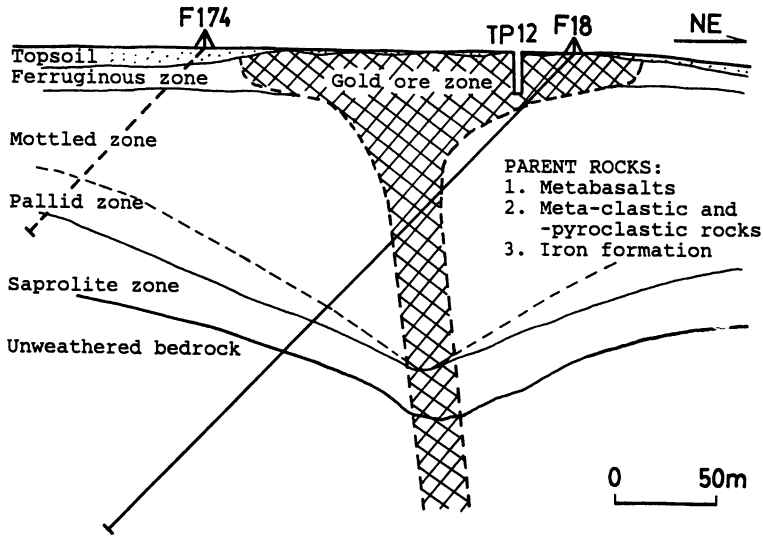

Figure 11. Schematic cross-section of the Igarapé Bahia lateritic gold deposit. Shaded areas represent gold ore zone which is developed on a near-vertical hydrothermally mineralized breccia zone (from Zang and Fyfe (*105*)).

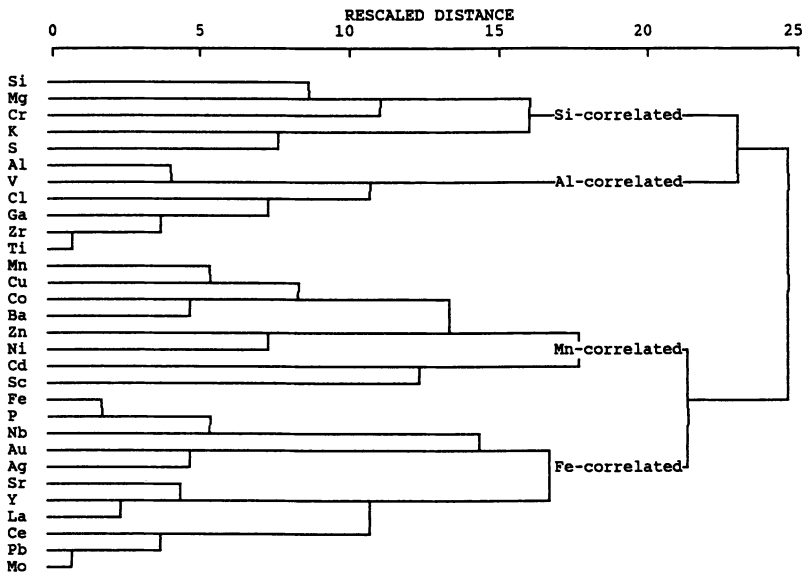

Figure 12: Dendogram of rescaled distance between chemical elements, showing Fe-, Mn-, Al-, and Si-correlated elements.

During incipient weathering Cu, Zn and Cd released from sulfides may be precipitated as carbonates (Cu also as native copper) or adsorbed by Fe-oxides (CuO 4.09 wt%) and Mn-oxides (CuO 2.09 wt%). As weathering proceeds the native copper and carbonates are dissolved and leached while some adsorbed elements are retained. Copper may replace Fe in the goethite lattice (*115*). Both Ni and Co can be enriched in Mn-oxides (CoO 1.47 wt%). It is well known that Ni occurs as an hydrated silicate (garnierite) in lateritic deposits. In this profile, however, only small amounts of Ni-carbonates were observed in fractures of the saprolite zone. Nickel is also found to be concentrated in goethite (NiO 0.09 wt%). The association of Ni with goethite was also reported in other laterite profiles (*116,117*). Cobalt has also been suggested to replace Fe^{3+} in Fe-oxides (CoO 0.18 wt%) (*118*). This correlates well with McKenzie (*119*) who noted that Mn-oxides contain relatively large amounts of Co, Ni and Cu, while Burns (*120*) suggested that Co coexists in Mn-nodules as Co^{3+} substituting for Mn^{4+}.

Al-Correlated Elements. Several elements, including Al, Ga, Cl, V, Ti, Zr are shown to be enriched in the mottled zone. Among these elements Ga probably replaces Al^{3+} in gibbsite and kaolinite. Titanium and Zr are frequently used as index elements to evaluate mobilities of other elements and calculate quantity of rocks consumed in weathering processes. In our profile, Ti and V are mainly present in relict ilmenite, whereas Zr occurs in zircon. Mobilities of Ti and Zr during intense weathering are also documented by Kronberg et al. (*100*), Zeissink (*116*) and Tampoe (*113*). The calculation, however, can not be applied to laterisation processes. Chlorine is readily leached out when the parent rock is weathered. The enrichment of Cl in the mottled zone is probably due to atmospheric addition rather than from weathering of parent rocks, as suggested by Kronberg et al. (*95*). Therefore, the association of Cl with Al could reflect porosity of the laterite profile, especially in the mottled zone.

Si-Correlated Elements. These elements include Si, Mg, K, Cr and S and are characterized by a gradual leaching from the profile as weathering proceeds, such that their concentrations decrease from the base to the top of the profile. Both Mg and K can be strongly enriched in smectite in the saprolite zone during incipient weathering, but are eventually leached out when smectite is replaced by kaolinite. Chromium is mainly enriched in silicates of parent rocks, such as chlorite (Cr_2O_3 0.12 wt%) and biotite (Cr_2O_3 0.23 wt%). It is, however, dissolved as the silicates are weathered. Chromium can be dissolved as $CrOH^{2+}$ under acid conditions at 25°C and 1 atm. (*121*). Sulfur is leached during sulfide dissolution.

Copper Dynamics in Two Profiles from the Carajás Mineral Province. In the Cu-mineralized area of the Carajás region two weathering profiles that developed in contrasting rock types were investigated. One profile, developed in silicate rocks, contained complex clay minerals at the base, an intermediate kaolinitic zone and an upper iron-rich zone. The second profile developed in iron-rich silicate and

oxide phases. In the latter, weathering proceeded slowly and was confined mainly to fissures extending tens of meters into the weathered zone. Because physical and mineralogical interactions, such as clogging of fissure systems by expanding clays, had reduced leaching and mineral alteration, there was extensive preservation of original mineralogy and retention of elements (e.g., Mg and Ca) that are normally rapidly leached.

The chemical dynamics of Cu in these profiles was studied using a suite of extractive techniques as well as bulk and surface analyses. The differences in styles of Cu partitioning gives some insight into the complexity of element partitioning as weathering proceeds. In the iron-rich profile, the style and extent of weathering appeared to be controlled by the kinetics of hematite (Fe_2O_3) alteration, with Cu hosted primarily in the fissure system (mainly in oxide and sulfide phases), while some Cu was associated with iron silicate phases (nontronite). In the silicate-rich profile only a small fraction of Cu was exchangeable. It appeared that Cu was immobilized in amorphous and crystalline iron oxide phases (ferrihydrite and goethite respectively) through surface complexation, followed by incorporation into bulk precipitates. Microscale observations in samples from both profiles also indicated the possible influence of microbial activity.

Conclusions

Rivers transport most of the materials which enter the oceans, yet our knowledge of the processes influencing their chemical composition remains inadequate. Much of what is known has been based on a compilation of data from extremely diverse sources. However, the inconsistencies suffered by fragmented data can be overcome through the study of large river systems which encompass a range of geological, climatic, and ecological variability to permit study of the concomitant effects determining river chemistry on a continental scale. Unfortunately, the difficulty encountered with most river basins is that much of their catchment has been influenced by man through agricultural and pastoral activities, industry, logging, hydroelectric projects, and settlement. The Amazon Basin, however, provided (by today's standards) an unusually ideal study area primarily because much of it remains largely undisturbed.

This study considered some of the influences which effect not only the source of solutes to Amazonian river systems, but also some of the factors which control the distribution of metals within their water columns and sediments. Without question, the largest source of metals to the river systems has proven to be weathering of the substrate lithology in source regions and within the erosional regime. Weathering not only governs the distribution of major elements and trace metals, but it also determines the concentration of organic matter in the river and the activity of microbial populations. These factors have proven to be of profound implication since organic material, both cellular and non-cellular, were shown to partially control the concentration of dissolved metals in both solute-rich rivers and solute-deficient rivers, respectively.

The preliminary results detailed above provide support for the proposition that it should be possible to obtain a record of vegetation change in the Amazon Basin from the carbon-isotope composition of terrestrial biomarker compounds extracted from marine sediments off the mouth of the river. The advantage of this approach is that it will yield a complete record from at least the last glacial maximum, and one which will be a record of large-scale changes in vegetation integrated across the entire basin.

It is clear that the detailed soil and water chemistry of the region and the stable isotope systematics provide indicators of the agricultural and mineral resource potential of this vast region and the climate history that has influenced the Amazon Basin. Recent data also shows that the chemistry and physical state and complexity of the weathered materials can only be explained by consideration of specific processes involving microorganisms. From surface to depths of 100's of meters, the weathered rocks are porous and permeable and obviously host living organisms. Modern observations show that the biosphere can extend to depths of several kilometers.

In Amazonia, humid climates and tectonic quiescence over millions of years have resulted in a high degree of partitioning of chemical elements in surface soils and sediments. The significant variation in the fate of elements at profile and regional scales underscores the influence of biological, physical and geological processes on chemical weathering pathways.

Literature Cited

1. Villa Nova, N.A.; Salati, E.; Matsui, E. *Acta Amazonica* **1976**, *6*, 215-228.
2. Meade, R.H.; Nordin, C.F.; Curtis Rodrigues, F.M.C.; Do Vale, C.M. *Nature*, **1979**, *278*, 161-163.
3. Meade, R.H.; Dunne, T.; Richey, J.E.; Santos, de U.M.; Salati, E. *Science* **1985**, *228*, 488-490.
4. Sioli, H. *Hydrobiol.* **1950**, *43*, 267-283.
5. Hedges, J.I.; Clark, W.A.; Quay, P.D.; Richey, J.E.; Devol, A.H.; Santos, U. de M.. *Limnol. Oceanogr.* **1986**, *3*, 717-738.
6. Leenheer, J.A. *Acta Amazonica* **1980**, *10*, 513-526.
7. Ertel, J.R.; Hedges, J.I.; Devol, A.H.; Richey, J.E.; Ribeiro, M.N.G. *Limnol. Oceanogr.* **1986**, *31*, 739-754.
8. Sioli, H. *The Amazon and its Main Affluents: Hydrography, Morphology of the River Courses, and River Types.* In *The Amazon*; Sioli, H., Ed.; W. Junk, Dordrecht, 1984; pp 127-166.
9. Raimondi, A. *Aguas Potables del Perù*. F. Masias, Lima, **1884**, pp. 127-134.
10. Katzer, F. *Wiss. Math. naturw.* **1897**, *17*, 1-38.
11. Sioli, H. *Amazoniana* **1968**, *1*, 267-277.
12. Sioli, H. *Tropical Rivers as Expressions of Their Terrestrial Environments.* In *Tropical Ecological Systems. Trends in Terrestrial and Aquatic Research;* Golley, F.B;. Medina, E., Eds.; Springer: New York, 1975; pp 275-288.

13. Stallard, R.F.; Edmond, J.M.. *J. Geophys. Res.* **1983**, *88*, 9671-9688.
14. Gibbs, R.J. *Science* **1970**, *170*, 1088-1090.
15. Gibbs, R.J. *Geochim. Cosmochim. Acta* **1972**, *36*, 1061-1066.
16. Gibbs, R.J. *Science* **1973**, *180*, 71-73.
17. Gibbs, R.J. *Geol. Soc. Amer. Bull.* **1977**, *88*, 829-843.
18. Stallard, R.F. *Eos* **1978**, *59*, 276.
19. Furch, K.; Junk, W.J.; Klinge, H. *Acta Cient. Venez.* **1982**, *33*, 269-273.
20. Furch, K. *Water Chemistry of the Amazon Basin: the Distribution of Chemical Elements Among Freshwaters*. In *The Amazon*; Sioli, H., Ed; Junk, W., Dordrecht, 1984; pp 167-200.
21. Fittkau, E.J.; Irmler, U.; Junk, W.J.; Reiss, F.; Schmidt, G.W.. *Productivity, Biomass, and Population Dynamics in Amazonian Water Bodies*. In *Tropical Ecological Systems: Trends in Terrestrial and Aquatic Research*.; Golley, F.B.; Medina, E., Eds.; Springer: New York, 1975; pp 289-311.
22. Konhauser, K.O.; Fyfe, W.S.; Ferris, F.G.; Beveridge, T.J. *Geology* **1993**, *21*, 1103-1106.
23. Fairbridge, R.W. *Encyclopedia of Earth Sciences Series*; Van Nostrand and Reinhold, New York, 1972, vol. 1VA; 1321 pp.
24. Taylor, S.R.; McLennan, S.M.. *The Continental Crust: its Composition and Evolution;* Blackwell Scientific Publications: Oxford, 1985; 312 pp.
25. Konhauser, K.O.; Fyfe, W.S.; Kronberg, B.I. *Chem.Geol.* **1994**, *111*, 155-175.
26. Leonardos, O.H.; Fyfe, W.S.; Kronberg, B.I. *Chem. Geol.* **1987,** 60, 361-370.
27. Stallard, R.F. *Weathering and Erosion in the Humid Tropics*. In *Physical and Chemical Weathering in Geochemical Cycles;* Lerman, A.; Meybeck, M., Eds; Kluwer Academic: Dordrecht, 1988**;** pp 225-246.
28. Gibbs, R.J. *Geol. Soc. Amer. Bull.* **1967**, *78*, 1203-1232.
29. Shaw, A. *Mining Magazine, August* **1990**, 90-97.
30. Fyfe, W.S. *Episodes* **1989**, *12*, 249-254.
31. Berner, E.K.; Berner, R.A. *The Global Water Cycle;* Prentice-Hall: New Jersey, 1987.
32. Fletcher, M. *Effect of Solid Surfaces on the Activity of Attached Bacteria*. In *Bacterial adhesion*; Savage, D.C; Fletcher, M., Eds;. Plenum; New York, 1985; pp 339-362.
33. Costerton, J.W.; Cheng, K.J.; Geesey, G.G.; Ladd, T.I.; Nickel, J.C.; Dasgupta, M.; Marrie, T.J. *Ann.Rev. Microbiol.* **1987**, *41*, 435-464.
34. Shimp, R.J.; Pfaender, F.K. *Appl. Environ. Microbiol.* **1982**, *44*, 471-477.
35. Neihof, R.A.; Loeb, G.I. *Limnol Oceanogr.* **1972**, *17*, 7-16.
36. Beveridge, T.J.; Murray, R.G.E. *J. Bacteriol.* **1980**, *141*, 876-887.
37. Ferris, F.G.; Beveridge, T.J. *FEMS Microbiol. Lett.* **1984**, *24*, 43-46.
38. Beveridge, T.J. *Can. J. Microbiol.* **1978**, *24*, 89-104.
39. Beveridge, T.J.; Murray, R.G.E. *J. Bacteriol.* **1976**, *127*, 1502-1518.
40. Mullen, M.D.; Wolf, D.C.; Ferris, F.G.; Beveridge, T.J.; Flemming, C.A.; Baily, G.W. *Appl. Environ. Microbiol.* **1989**, *55*, 3143-3149.

41. Kuyucak, N.; Volesky, B. *Biorecovery* **1989**, *1*, 219-235.
42. Mann, S. *Biomineralization in Lower Plants and Animals-Chemical Perspectives*. In *Biomineralization in Lower Plants and Animals;* Leadbeater, B.S.C.; Riding, R., Eds.; The Systematics Association. Special Volume No. *30*, Clarendon: Oxford, 1986, pp 39-54.
43. Beveridge, T.J.; Fyfe, W.S. *Can. J. Earth Sci.* **1985**, *22*, 1893-1898.
44. Sullivan, C.W.; Volcani, B.E. *Silicon in the Cellular Metabolism of Diatoms*, In *Silicon and Siliceous Structures in Biological Systems;* Simpson, T.L.; Volcani, B.E., Eds.; Springer: New York, 1981; pp. 15-42.
45. Simkiss, K. *The processes of Biomineralization in Lower Plants and Animals*. In: *Biomineralization in Lower Plants and Animals*; Leadbeater, B.S.C.; Riding, R.; The Systematics Association. Special Volume No. 30, Clarendon Press: Oxford, 1986; pp 19-38.
46. Ferris, F.G.; Beveridge, T.J.; Fyfe, W.S. *Nature* **1986** *320*, 609-611.
47. Wada, K. *Amorphous Clay Minerals-Chemical Composition, Crystalline State, Synthesis, and Surface Properties*. In Developments in Sedimentologoy; van Olphen, H.; F. Veniale, F., Eds.; *Proceedings of the V11 International Clay Conference*. Elsevier Scientific.; Amsterdam, 1981, Vol. 35 pp 385-398.
48. Nadeau, P.H. *Clay Miner.* **1985**, *20*, 499-514.
49. Beveridge, T.J.; Meloche, J.D.; Fyfe, W.S.; Murray, R.G.E. *Appl. Environ. Microbiol.* **1983**, *45*, 1094-1108.
50. Wissmar, R.C.; Richey, J.E.; Stallard, R.F.; Edmond, J.M. *Ecology* **1981**, *62*, 1622-1633.
51. Konhauser, K.O.; Fyfe, W.S. *Energy Sources* **1993**, *15*, 3-16.
52. Jordan, C.F. *Soils of the Amazon Rainforest.* In *Amazonia*;. Prance, G.T.; Lovely, T.E., Eds.; Pergamon Press: Oxford, 1985; pp 83-94.
53. Lack, T.J. *Freshwat. Biol.* **1971**, *1*, 213-224.
54. Schelske, C.L.; Stoermer, E.F. *Science* **1971**, *173*, 423-424.
55. Konhauser, K.O.; Mann, H.; Fyfe, W.S. *Geology.* **1992**, *20*, 227-230.
56. Reynolds, C.S. *Diatoms and the Geochemical Cycling of Silicon.* In *Biomineralization in Lower Plants and Animals;* Leadbeater, B.S.C.; Riding, R., Eds.; Systematics Association Special *Volume 30*. Claredon: Oxford, 1986, pp 269-289.
57. Hesse, R.. *Origin of Chert: Diagenesis of Biogenic Siliceous Sediments*. In *Diagenesis*;. Mcllreath, I.A.; Morrow, D.W., Eds.; Geological Association of Canada, Geoscience Canada Reprint Series 4, 1990; pp 227-251.
58. Hein, J.R.; Scholl, D.W.; Barron, J.A.; Jones, M.G.; Miller, J. *Sedimentology* **1978**, *25*, 155-181.
59. Williams, L.A.; Parks, G.A.; Crerar, D.A. *J. Sediment Petrol.* **1985**, *55*, 301-311.
60. Sigleo, A.C. *Geochim. Cosmochim. Acta* **1978**, *42*, 1397-1405.
61. Schlesinger, W.H.; Melack, J.M. *Tellus* **1981**, *33*, 172-187.
62. Lamar, W.L. *U.S. Geol. Surv. Prof. Paper 600-D*, D24-D29 **1986**.

63. Reuter, J.H.; Perdue, E.M. *Geochim. Cosmochim. Acta* **1977**, *41*, 325-334.
64. Degens, E.T. *Mitt. Geol. Palaont. Inst. Univ. Hamburg SCOPE/UNEP Sonderb* **1982**, *52*, 1-12.
65. Rashid, M.A.,. Absorption of metals on sedimentary and peat humic acids. *Chem. Geol.* **1974**, *13*, 115-123.
66. Beck, K.C.; Reuter, J.H.; Perdue, E.M.. *Geochim. Cosmochim. Acta* **1974**, *38*, 341-364.
67. Bowen, H.J.M. *Environmental Chemistry of the Elements.*; Academic Press: London, 1979; pp 237-272.
68. Stumm, W.; Morgan, J.J. *Aquatic Chemistry*; Wiley-Interscience: New York, 1970.
69. Colinvauz, P.A. *Nature* **1989**, *340*, 188-189.
70. Crowley, T.J. *Nature* **1991**, *352*, 575-576.
71. Bigarella, J.J.; Andrade-Lima, D. de *Paleoenvironmental Changes in Brazil.* In *Biological Diversification in the Tropics.*; Prance, G.T., Ed.; Columbia University Press: New York, 1982; pp 27-40.
72. Absy, M.L.; Clef, A.; Fournier, M.; Martin, L.; Servant, M.; Siffedine, A.; Ferreira da Silva, M.; Soubies, S.; Suguio, K.; Turcq, B.; Van der Hammen, T. *Mise en Evidence de Quatre Phases d'ouverture de la Forêt Dense dans le sud-est de l'Amazonie au cours des 60000 Derniéres Années. Premiere Comparaison avec d'autres Régions Tropicales.*; C.R. Acad.Sci. Paris, 1991; 312, pp 673-678.
73. Van der Hammen, T. *J. Biogeogr.* **1974**, *1*, 3-26.
74. Räsänen, M.E.; Salo, J.S.; Kalliola, R.J. *Science* **1987**, *238*, 1398-1401.
75. Bush, M.B.; Colinvaux, P.A.; Weimann, M.C.; Piperno, D.R.; Liu, K-B. *Quat. Res.* **1990**, *34*, 330-345.
76. Nelson, B.W.; Ferreira, C.A.C.; da Silva, M.F.; Kawasaki, M.L. *Nature* **1990**, *345*, 714-716.
77. Smith, B.N.; Epstein, S. *Plant Physiolo.* **1971**, *47*, 380-384.
78. Bird, M.I.; Fyfe, W.S.; Pinheiro-Dick, D.; Chivas, A.R. *Global Biogeochem. Cycles* **1992**, *6*, 293-306.
79. Cai, D.-L.; Tan, F.C.; Edmond, J.M. *Estuarine Coastal Shelf Sci.* **1988**, *26*, 1-14.
80. Mariotti, A.; Gadel, F.; Giresse, P.; Kinga-Mouzeo *Chem. Geol.* **1991**, *86*, 345-357.
81. Bird, M.I.; Giresse, P.; Chivas, A.R. *Chem. Geol.* **1993**, *107*, 211.
82. Showers, W.J.; Angle, D.G. *Continent. Shelf. Res.* **1986**, *6*, 227-244.
83. Kolattukudy, P.E. *Chemistry and Biochemistry of Natural Waxes;* Elsevier: New York, 1976.
84. Van Fleet, E.S.; Quinn, J.G. *Deep Sea Res.* **1979**, *26A*, 1225-1236.
85. Reiley, G.; Collier, R.J.; Jones, D.M.; Eglington, G.; Eakin, P.A.; Fallick, A.E. *Nature* **1991**, *352*, 425-427.
86. Hayes, J.M.; Freeman, K.H.; Popp, B.N.; Hoham, C.H. *Org.Geochem.* **1990**, *16*, 1115-1128.

87. Ertel, J.R.; Hedges, J.I. *Geochim Cosmochim. Acta.* **1985**, *49*, 2097-2107.
88. Hedges, J.I.; van Geen, A. *Mar. Chem.* **1982**, *11*, 43-54.
89. Hartley, R.D.; Buchan, H. *J. Chromatogr.* **1979**, *180*, 139-143.
90. Benner, R.; Fogel, M.L.; Sprague, E.K.; Hodson, R.E. *Nature* **1987**, *329*, 708-710.
91. Kronberg, B.I.; Benchimol, R.E.; Bird, M.I. *Interciencia* **1991**, *16*, 138-141.
92. Kronberg B.I.; Nesbitt, H.W. *J. Soil Sci.* **1981**, *32*, 453-459.
93. Garrels R.M.; Mackenzie, F.T. *Evolution of Sedimentary Rocks;* W.W. Norton: New York, 1971.
94. Livingstone, D.A.,. Chemical Composition of Rivers and Lakes. *U.S. Geol. Surv. Prof. Pap. 440-G*, **1963**, pp 1-63.
95. Kronberg, B.I.; Nesbitt, H.W.; Fyfe, W.S. *Chem. Geol.* **1987**, *60*, 41-49.
96. Stallard, R.F.; Edmond, J.M. *J. Geophys. Res.* **1981**, *86;* 9844-9858.
97. Kronberg B.I.; Nesbitt, H.W.; Lam, W.W. *Chem.Geol.* **1986**, *54*, 283-294.
98. Bird, M.I.; Longstaffe, F.J.; Fyfe, W.S.; Kronberg, B.I.; Kishida, A. *Geophysical Monograph 78*, American Geophysical Union. **1993**.
99. Kronberg, B.I.; Couston, J.; Stilianidi, B.; Fyfe, W.S.; Nash, R.A.; Sugden, D. *Econ. Geol.* **1979**, *74*, 1869-1875.
100. Kronberg, B.I.; Fyfe, W.S.; McKinnon, B.J.; Couston, J.F.; Stilianidi Filho, B.; Nash, R.A. *Chem. Geol.* **1982**, *35*, 311-320.
101. Stark, N.M.; Jordan, C.F. *Ecology* **1978**, *59*, 434-437.
102. Newell, R.C. *The Amazonas Forest and the Atmospheric General Circulation.* In *Man's Impact on Climate;* Kellog, W.H.; Robinson, G.D., Eds.; MIT Press: Boston, **1971;** pp 457-459.
103. Molion, L.C.B.; Betancurt, J.J.U. *Land Use and Agrosystem Management in Humid Tropics.* In *Woodpower: New Perspectives in Forest Usage;*.Talbot, J.J.; Swanson, W., Eds.;. Pergamon: Oxford, 1981; pp 119-128.
104. Melfi, A.J.; Trescases, J-J.; Carvalho, A.; Barros de Oliveira, S.M.; Ribeiro Filho, E.; Laquintine Formoso, M.L. *Sci. Geol. Bull.*, **1988**, *41*, 5-36.
105. Zang, W.; Fyfe, W.S. *Econ. Geol.* **1993**, *88*, 1768-1779.
106. Zang, W. Ph.D. Thesis, University of Western Ontario, Canada, **1993**
107. McFarlane, M.J. *Laterite and Landscape;* Academic Press: London; 1976.
108. Tardy, Y.; Nahon, D. *Amer. J. Sci.* **1985**, *285;* 865-903.
109. Nahon, D.B. *Evolution of Iron Crusts in Tropical Landscapes.* In *Rates of Chemical Eeathering of Rocks and Minerals;*. Colman, S.M.; Dethier, D.P. Eds.; Academic: Orlando, 1986; pp 169-191.
110. Nickel, E.H. *Geochem. Explor* **1984**, *22*, 239-264.
111. Zang, W.; Fyfe, W.S.; Barnett, R.L. *Mineral. Mag,* **1992**, *56*, 47-51.
112. Melfi, A.J.; Cerri, C.C.; Kronberg, B.I.; Fyfe, W.S.; McKinnon, B. *J. Soil Sci.* **1983**, *34*, 841-851.
113. Tampoe, T.J. *Ph.D. Thesis*, University of Western Ontario, Canada. 1989.
114. Jones, L.H.P. *J. Soil. Sci.* **1957**, *8*, 313-327.
115. Lesarge, K.G. M.Sc. Thesis, University of Western Ontario, Canada, 1991.
116. Zeissink, H.E. *Chem.Geol.* **1971**, *7*, 25-36.

117 Schellmann, W. *Geochemical Principles of Lateritic Nickel Ore Formation.* Proc. 2nd Int. Semin. on Laterization Processes. Univ. São Paulo, São Paulo, Brazil, 1983; pp 119-135.
118. Topp, S.E.; Salbu, B.; Roaldset, E.; Jorgensen, P. *Chem. Geol.* **1984**, *47*, 159-174.
119. McKenzie, R.M. *Australian J. Soil Res.* **1967**, *5*, 235-246.
120. Burns, R.G. *Geochim. Cosmochim. Acta* **1976**, *40*, 95-102.
121. Brookins, D.G. *Eh-pH Diagrams for Geochemistry.*; Springer: Berlin, 1988.

RECEIVED December 28, 1994